Response to Reviewer RC2 – Prof. Christian Schoof

Egusphere-2024-1052 Article

Author Responses in Blue

I thank Prof. Schoof for a detailed and insightful review!

Overview

The paper builds a unified variational formulation for Stokes flow and the somewhat misnamed Blatter-Pattyn model for ice flow. To get the trivia out of the way, I will call this the Herterich-Blatter-Pattyn model from this point onwards. History may be written by the winners, and Herterich clearly hasn't been one of them, *but* the first instance of the Herterich-Blatter-Pattyn model being formulated was (to my knowledge) the following paper:

- Herterich, K. 1987. On the flow within the transition zone between ice sheet and ice shelf, *in* Dynamics of the West Antarctic Ice Sheet. Proceedings of a workshop held in Utrecht, May 6–8, 1985, pp.!185–202. D. Reidel, Dordrecht,

This predates the commonly used Blatter (1995) and Pattyn (2003) references by eight and sixteen years, respectively. If we're going to fall into the trap of naming things after people, we probably owe it to ourselves to do that accurately. Not that I've been able to convince anyone of this point so far.

I was not familiar with this reference (I doubt many people are) so I looked into this model to compare it to the BP model. It turns out that the Herterich model is NOT equivalent to the Blatter-Pattyn model. Instead, it is the same as the BP+ approximation that's described in §6.2.1. I've attached a derivation of this result at the end after these responses, in an Appendix, and I've also added a short discussion in §6.2.1 regarding this. Needless to say, I will not be changing the name of the Blatter-Pattyn model. Thank you for pointing out this reference.

Back to the present. It took me a bit of effort in stripping away detail and side notes to understand that the primary advance of the paper is a numerical formulation in which one can dynamically switch between the simpler Herterich-Blatter-Pattyn and the more complete Stokes flow model. The latter applies to flows with arbitrary aspect ratios and abrupt changes in boundary conditions, while the former requires a "shallow" flow.

At face value, such a "switchable" model makes a lot of sense, since ice sheet flow is shallow in most places, but often contains boundary layers (at ice divides, ice stream margins, grounding lines etc) where the Stokes equations must be solved. The present paper uses the variational structure of both models to create a unified formulation, by re-writing the Lagrangian for the Stokes equations so that it takes the form of the Herterich-Blatter-Pattyn Lagrangian with a few extra terms retained. The unified formulation then consists of introducing a flag that activates or deactivates these Stokes correction terms. This is an intriguing idea and deserves to be published. I am not entirely convinced that

August 27, 2024

You are right, this is an important advance introduced in the paper. However, I also want to point out the additional innovations, such as the new approximations that improve on Blatter-Pattyn and the introduction and use of grids, such as P1-E0, that permit the solution of the continuity equation for $w(u,v)$. To this effect, I have rewritten Section 8 (I hope you don't mind that I used some of your words to do this).

This is an intriguing idea and deserves to be published. I am not entirely convinced that *The Cryopshere* is the right vehicle as there are a number of technical issues that deserve more thorough scrutiny; *Geoscientific Model Development* would have seemed a more appropriate journal in the EGU stable to use, but really I would have been inclined to go with something like *J. Comp. Phys.*.

I did consider Geosci. Model Dev. and J. Comp. Phys. Unfortunately, I was not able to comply with GMD's code availability requirement. JCP did not seem appropriate because the paper is too specialized to ice sheet modeling.

As far as I can tell, the modified Stokes Lagrangian does not alter the saddle point strucutre of the Stokes flow problem (in the sense that the solution maximizes the modified Stokes functional with respect to $\tilde{p}$ and minimizes with respect to $\boldsymbol{u}$). Still, the modified Stokes Lagrangian is a fairly ugly object that obscures the natural symmetries of the original Stokes flow Lagrangian and introduces a much larger null space to the elliptic operator. For the usual Stokes flow Lagrangian, that null space consists of rigid body rotations modulo any such motions that are precluded by the boundary conditions (by way of restrictions on the space of admissible functions). In the modified Stokes Lagrangian of the present paper, the vertical velocity w can be changed by adding an arbitrary function of the vertical coordinate z only while leaving the elliptic part of the Lagrangian uchanged; such functions of z are then penalized through the incompressibility constraint.

That ugliness appears to be an unavoidable part of a unified formulation. It does however mean that you would probably not choose to use the modified Lagrangian for the analysis of general Stokes flow problems, except to unify the Stokes and Herterich-Blatter-Pattyn problem computationally. The paper can probably streamlined by focusing on that aspect at the exclusion of some of the more peripheral commentary, and the title of the paper could probably be made more informative.

You are quite right. I do not advocate the transformed Stokes formulation for the solution of general Stokes problems. As presented in the paper I view it primarily as a means to (a) "unify the Stokes and Blatter-Pattyn problem computationally", §6.1, and (b) as a means of developing new approximations that improve on BP, §6.2. On the other hand, the transformed Stokes model can perform better computationally than the standard Stokes model. Section 5 compares some computational results for the standard and transformed Stokes formulation. Fig. 3 shows that the transformed

model is more accurate than the standard model for Test B (no-slip) calculations at all resolutions. However, this is probably a fortuitous result because the two cases in the Test D* (frictional sliding) calculations show similar accuracy.

In terms of pursuing that unification of Stokes and Herterich-Blatter-Pattyn models, there are two significant issues that I can see:

1. While the variational formulation of the Stokes flow problem *is* a saddle point problem, the same is not true of the Herterich-Blatter-Pattyn problem. The latter naturally wants to be solved as an unconstrained minimization problem, with the incompressibilty condition solved a posteriori for the vertical velocity component w. Enforcing incompressibility through a Lagrange multiplier as part of the variational formulation leads to problems that occupy most of the technical material in the paper: unlike the modified Stokes Lagrangian, the elliptic part of the Herterich-Blatter-Pattyn Lagrangian does not contain w at all, which must instead be solved for through the (hyperbolic) incompressibility condition alone — for which the standard function spaces used in Stokes flow solvers are unsuitable. This is perhaps unsurprising, as the standard function spaces used in finite elements are problematic for hyperbolic equations, and discontinuous basis functions (as used in discontinuous Galerkin methods) might be preferable for w in the Herterich-Blatter-Pattyn problem; they might at least alleviate issues such as $\nabla \cdot \boldsymbol{u} = 0$ being an overdetermined problem if we assume that $\boldsymbol{u}$ is represented by P1 basis functions, which work well for the force balance part of the Herterich-Blatter-Pattyn problem.[1]

   The main challenge identified in the paper (which motivates the choice of those P1–E0 soaces, and the others discussed in sections 6,7 and appendix C) is to make sure that the choice of basis functions for the "Blatter-Pattyn system" (that is, the Blatter-Pattyn equations and the incompressibility condition) can also be used for the modified Stokes system. Unfortunately, I think that there are some issues with how this has been addressed in the paper, and I suspect that there is a misunderstanding of what the inf-sup ("LBB") condition really does. More on this below.

---

[1] By contrast, the "P1-E0" spaces advocated here go in a different direction: w is still represented by piecewise linear, and therefore continuous, basis functions, but the incompressibility constraint is weakened through the choice of a "coarser" basis function for the Lagrange multiplier that enforces incompressibility, averaging over two adjacent elements.

I don't have a quarrel with what is said here so I will postpone a response to where the inf-sup condition is discussed later.

August 27, 2024

2. More practically, I am not convinced that the method developed here will be adopted widely. Consider this: unlike its depth-integrated variants developed by Richard Hindmarsh, the Herterich-Blatter-Pattyn requires a three-dimensional domain to be resolved. This leads to a large number of computational degrees of freedom. In fact, the only advantage relative to a Stokes flow model is that there are fewer variables to be solved for in *the same* computational domain, as you can solve for (u, v) using the elliptic solver, and the compute w and p *a posteriori* if required. As far as I can tell, the Seroussi et al (2012, cited in the manuscript) tiling method makes use of that. The method proposed here, of solving for (u, v, w, p) using the same basis functions for both models without explicitly using the simpler structure of the Herterich-Blatter-Pattyn model, seems to get rid of that last advantage. Which begs the question, why bpther, given that the Stokes model is preferable in terms of the physics it represents. Unfortunately, the last paragraph of the conclusion puts paid to any hope that the paper might address whether the new approach is actually going to be computationally competitive.

I think this comment refers to the use of the transformed model in a "unified formulation". There is no question that the BP model is much cheaper, although less accurate, than a full-Stokes model. This is the reason why BP rather than Stokes is used in several production code packages (e.g., ISSM, MALI, CISM). Depth-integrated models are still cheaper but even less accurate. The approximations presented in §6.2 are at the high end of this scale; they are more accurate and more expensive than BP but still cheaper than Stokes. There is a tradeoff between accuracy and computational cost so a choice has to be made depending on the application.

I would not say that the standard Stokes formulation is preferable in terms of the physics it represents. The two formulations represent exactly the same physics and provide the same solutions to a given problem. They are, after all, mathematically related by a transformation. They differ, if at all, by their numerical behavior.

The adaptive switching example of §6.1 makes use of the "Blatter-Pattyn system", i.e., solving for (u, v, w, p), for simplicity and just to illustrate the method, even though this is more expensive than it needs to be. In a practical application it should be possible to switch to using the Blatter-Pattyn model instead, i.e., solving for (u, v), and coupling to the Stokes model using $p = 0$ and $w = w(u, v)$ at the interface, even though this would involve more complicated programming. I have added some sentences to this

August 27, 2024

effect in the paper.

To follow up on the first point above, I am concerned that appendix D is misleading. Apologies if this gets a little long below; I am not as much of an expert at this as I'd like to be, so it took me a bit more explanation. My understanding of the inf-sup or Ladyzhenskaya-Babuška-Brezzi condition for Stokes flow problems is the following. Take the Hessian matrix in (55) of the present paper

$$M = \begin{pmatrix} A & B \\ B^T & 0 \end{pmatrix} \qquad (1)$$

and we have to solve $Au + Bp = f$, $B^Tu = 0$ where f is the relevant residual of the Stokes equations. A is positive semi-definite, which makes the solution of this problem (if it exists) equivalent to a saddle point: to find

—

—

—

Long discussion of inf-sup condition

—

—

—

I hope I have been clear to say that I may be wrong. If I am, the text of the paper should be more explicit about the technical issues that I have raised; it's currently fairly vague in spelling out what the "LBB" (inf-sup) condition actually is, what it does, and whether the basis functions described in sections 6–7 and appendix C satisfy the inf-sup condition. (Also, if you're going to introduce a concept like that, please spell out what the acronym "LBB" stands for before using it, and maybe cite the original places where it comes from.)

---

[3]since I would otherwise have $B(v_h, q_h) = 0$ for all v_h and some q_h

[4]There is another issue in play here: the inf-sup condition provides sufficient conditions for a convergence, but not necessary ones. You might also decide that you don't care about convergence of the discretized pressure solution $\tilde{p}_h$, but only of u_h, which may conceivably relax the conditions you need to impose. I am not in a position to comment on that, however — you need a real expert reviewer.

I have eliminated Appendix D and rewritten Section 4 to bypass the difficult issue of the inf-sup condition. The inf-sup condition is relevant only so as to point out that the standard and transformed Stokes models are subject to it and that one must use one of the many inf-sup-stable elements available in the literature in the discretization.

I hope I have made it clear that the inf-sup condition does not apply to problems using elements satisfying the "solvability condition" because they are no longer constrained problems since incompressibility is built-in when using $w(u,v)$.

August 27, 2024

My other main points would be the following (partially elaborated under "specific points")

1. The notation in the paper is fairly idiosyncratic, which made it more time-consuming for me to follow various pieces. There is a mix of standard subscript notation, a very much nonstandard "round bracket around subscript means projection onto the horizontal plane" variant to subscript notation, and the use of explicit component

   notation as in equations (7), (28) and (35) to write scalar quantities that should really be denoted by contractions over subscripts. The paper makes enough assumption about the reader's level of mathematics that I would recommend streamlining this as I don't imagine much of an audience who will be helped rather than hindered by the nonstandard notation. In particular, I would discourage the round bracket notation in favour of a more standard projection operator: if P is the projection onto the horizontal plane, $P(v_1, v_2, v_3) = (v_1, v_2, 0)$, then you can simply replace a_i by $P_i(\boldsymbol{a})$ and retain summation over indices from 1 to 3. I say this even though the author has used it previously: the use of nonstandard notation it may make the paper harder to decipher for numerical analysts, who should really be encouraged to delve deeper into the theory relevant to the paper.
   The use of superscripts (s), (b_1) and (b_2) on surface normals is also redundant, as you specify the parts of the domain boundary to which the stated boundary conditions apply. Keep this as simple as possible, because it it certainly isn't simple.

   The second invariant was written in subscript notation, $\dot{\varepsilon}^2 = \dot{\varepsilon}_{ij}\dot{\varepsilon}_{ij}/2$, just before equations (7) and (28) but then expanded for clarity.

   I prefer using the nonstandard horizontal-index notation, i.e., $u_{(i)}$ vs $P_i(u)$, because it is more compact. However, I've added a sentence to clarify this in the paragraph following Fig. 1.

   I have removed superscripts on surface normals as per your suggestion. Thank you.

2. The paper is quite ungenerous to the prior literature. I can see the appeal of referencing only your own paper ("DPL" in the present case) as the default reference because you know its content extremely well, but many of the introductory concepts in this manuscript have been developed in other places, which remain uncited. That may put off other practicioners who should read this paper (and who might in fact get some sort of notification, alerting them to your paper if you were to cite them!). It's also unhelpful to any reader who wants to make sense of the field: the may conclude that, really, only DPL is relevant as a prior publication. In particular, I see almost no reference to the extensive numerical analysis literature on Herterich-Blatter-Pattyn and Stokes flow models in glaciology (except my ca. 2010 own effort in that direction, which does get a citation somewhere).

   I am happy to add additional or more appropriate references. Any suggestions?

August 27, 2024

3. The "Improved Blatter-Pattyn or BP+ Approximation" in section 6.2.1. I am unconvinced that it makes sense to include this in the present paper, unles you want to "patent" the idea for eternity. (Who knows, maybe someone will in future refer this approximation by someone else's name, the same fate that befell Herterich?) The reason why I am unconvinced is that this material further breaks the flow of the paper, without being robust. The supposedly improved approximation remains an *ad hoc*, partial retention of higher order terms in the Stokes flow model, higher order being in sense of the aspect ratio. There is no theoretical justification for doing that, as a partial retention of higher order terms in a model comes with no guarantee of a reduction in model error. In fact, it can make the model error worse. We do see a reduction in model error for the "BP+" model ("HBP+" / "D"?) in the single test that the "improved" model has been subjected to (ISMIP-HOM Test B, figure 9 of the manuscript). However, that is not really a robust demonstration of an "improved" model. It's also unclear whether the supposedly improved model is really competitive relative to solving the full Stokes model in terms of the tradeoff

between accuracy and computational effort. (See my second major point above.)

I wonder if this comment is relevant now that we understand that the BP+ approximation is the same as the Herterich model? I doubt that it's necessary to have a full scale analysis when introducing a new approximation. For example, the Blatter-Pattyn model did not have a scale analysis for 15 years until Schoof and Hindmarsh (2010).

Specific points

A number of specific points, some of which will replicate elements of what I've written above.

- p3, line 81: "finite element grid" — "grid" might be seen to imply regularity. "finite element basis functions"? I mean, closer scrutiny does indicate that the basis functions used here are restricted to quite regular meshes, so perhaps the terminology is not wrong here, but that required regularity actually needs to be discussed somewhere.

Changed "grids" to "discretizations"

- p3 line 84 "these two elements are so-named because they employ edge-based pressures" — I actually found that confusing. The basis function for pressure is not really defined on edges (since there are plenty of edges in the mesh that don't have a pressure defined on them). They are really P0 basis functions in which two adjacent triangles of the triangulation are assigned the same pressure.
  Also, to make it clear that you are inventing these basis functions, avoid the passive voice here. "I have named these E0 to indicate that pressure is defined on select element edges" or similar. It took me a while to realize that I would look in vain for references to these elements in the literature.

August 27, 2024

I have changed the wording as follows "these two elements are novel and are so-named because they employ pressures located on vertical grid edges"

- p 3 line 89 onwards " A conventional ice sheet Stokes model discretized on such a grid is numerically equivalent to an inherently stable positive-definite minimization (i.e., optimization) problem, as demonstrated in Appendix D. This is in contrast to the ubiquitous Stokes finite element practice of needing to use elements that satisfy the "inf-sup" or "LBB" condition for stability (see Elman et al., 2014, and the brief discussion in §4.3.1)." — This honestly confused me. If you're saying that current practice in solving the Stokes equations in ice sheet dynamics ("A conventional ice sheet Stokes model") is to use unconstrained optimization, then please provide a reference. It's very hard to do unconstrained optimization for Stokes flow as you need divergence-free basis functions. If you mean that *your new approach* is equivalent to constructing such a divergence-free basis, then say that instead. However, you really also need to show that the reduction of the single Newton iteration step to a problem for $(u_1, \ldots, u_N, w_1, \ldots, u_N)$ only in appendix D (taking the dimensionality argument for $\mathbf{M}_{WP}$ at face value) really is equivalent to a convergent solution (under mesh refinement) of the unconstrained Stokes optimization problem (that is, the problem in which the incompressibility constraint is directly imposed on admissible $\boldsymbol{u}$). I don't think this is entirely trivial, see also my discussion of the inf-sup criterion above. (Put this another way, for any set of basis functions that allows the problem to be solved, I must be able in principle to

  eliminate the discretized pressure variable in favour of retaining on the nodal values of velocity, even if I would not choose to do the matrix manipulations involved. By your logic, any such scheme should therefore be robust. Is that true?) I may be mistaken about what you're trying to say here, but it may therefore be worth finding a different way of saying it.

As mentioned on Page 5 of this response, I have eliminated Appendix D and rewritten Section 4 and I hope that this now addresses the issue. No, my approach is not equivalent to constructing divergence-free basis functions. In fact, I doubt that such a basis exists (Boffi et al. (2008), a new reference added in the paper). What I am trying to say is that given an arbitrary discrete horizontal velocity field (u) on a grid that satisfies the solvability condition (i.e., square, full rank matrix M_{WP}^T), I can always find an "incompressible" velocity field $(u, w(u))$. This, when substituted into a constrained functional (Jacobian?) for variables (u, w, p) converts it into an equivalent unconstrained functional for (u) alone. This is what I'm trying to say in the new Section 4.3.2. I have also reworded the end part of the Introduction to express this.

August 27, 2024

- p 4 line 116. $S = S_{B1} \cup S_{B2}$?

Changed

- p 4 line 121–123. See above re: notation.

- eqs (8), (10, (11), (13)–(15). The superscripts on your unit normals seem to be redundant. There is only one (outward-pointing) unit normal to each of these parts of the boundary.

Corrected, see Point 1 above.

- p 6 line 174, "f_i is a specified frictional sliding force vector." — f_i has the wrong units for a force. It's a traction, but why not just call it an interfacial shear stress? τ_i would probably be a more common symbol.

Changed throughout the paper except that I used the symbol to τ_i^S to avoid confusion with the stress tensor τ_{ij}.

- p6, line 170 "the simplest representation" — I beg to differ. There is a standard way of writing shear stress, as the traction $\Sigma_i = \sigma_{ij}n_j$ minus the normal component of traction $n_i \Sigma_j n_j$, or
$$(\delta_{ij} - n_i n_j)\sigma_{jk}n_k.$$
That is equation (71) in appendix A, and I think you'd be well advised to just use that (standard) form. (The point about weak solutions is surely that you never need to actually evaluate the shear stress itself from the stress tensor and the normal to the surface; you just need to know the constitutive relation, which here is just
$$(\delta_{ij} - n_i n_j)\sigma_{jk}n_k. = \beta u_i.$$
I think what the paper says isn't wrong, but manipulations don't seem they will help the unwitting reader, who is just wrapping their head around the basic model formulation. Especially at this point, where you haven't motivated your use of the bracketed indices at all yet, in terms of the mathematics you're doing.

- page 13, equation (32). As above, that is pretty ugly. I can't tell if there is a less confusing form, but might be worth trying.

You are right! The form I was using is computationally easier because it eliminates the complicated quantity $\tau_n = n_i \tau_{ij} n_j$, the normal component of the stress force. But if the discretization is based on a variational principle (or on a weak formulation) this is irrelevant because this quantity never needs to be explicitly calculated. One might as well eliminate Appendix A (shortens the paper!) and obtain the tangential frictional shear stress as in DPL (2010) or your expression above, except that I prefer to use the

August 27, 2024

deviatoric stress tensor as in the rest of the paper. Equations (11) and (32) have been updated.

- p 7 line 180 "...can easily be added" → "...can esaily be added to equation (10)"?

Done

- p 8 line 218 " Here we use z_b as a shorthand notation for $z_b(x,y)$' — this is surely redundant? Same on line 259.

Removed in both places.

- p 7 "(see DPL, 2010, for a fuller description of the variational principle applied to ice sheet modeling)" — you should refer to Chen, Q, M. Gunzburger and M. Perego. 2013. Well-posedness results for a nonlinear Stokes problem arising in glaciology. *SIAM J. Math. Anal.*, 45(5), 2710-2733. This is probably the most comprehensive analysis of Stokes flows with sliding in glaciology (and you'll find the relevant functional there, too, naturally).

Reference added

- p 7 line 200 "...(see Schoof, 2010, in connection with the Blatter-Pattyn model)" — I feel a little unfairly singled out here. There are earlier papers by Coling and Rappaz (MSAN, 1999), Glowinski and Rappaz (2003), Chow et al 92004) Rappaz and Reist (M3AS, 2005) that deserve an equal mention as having contributed to the analysis of the Herterich-Blatter-Pattyn model

I've inserted "as well as earlier references contained therein"

- p8 line 208 " As in DPL (2010), arguments enclosed in square brackets, here u_i , P, λ_i ,Λ , indicate those variables that are used in the variation of the functional." — this is an odd way of putting it. A functional is simply a mapping (or function) from some vector space (or perhaps an affine space) into the real numbers. So why not just say that you're enclosing the arguments of the functional (which is a function and therefore takes arguemnts like any other function![5]) in square brackets.

---

[5]Unless you insist that a function have to take arguments in $\mathbb{R}^n$ for some finite n.

I have rephrased it as "As in DPL (2010), arguments enclosed in square brackets, here $u_i, P, \lambda_i, \Lambda$, indicates those functions that are subject to variation as arguments of the functional ". Hope this helps.

- page 9 line 254"...as is done in the Blatter-Pattyn approximation (see DPL, 2010)."— is the apropriate reference not one of Herterich (1987), Blatter (1995) or Pattyn (2003(?

Yes, replaced by Pattyn (2003). I couldn't actually find it in Blatter (1995).

- page 12 line 296. It would be a good idea to explain the role of the flag parameters ξ and $\hat{\xi}$ earlier. I spent a page half guessing what they were.

August 27, 2024

The dummy variables are now explained directly below where they are introduced, i.e., right after equations (23)-(28).

- p 8 line 210 onwards. I don't think this correct, or at least, it seems misleading. In my understanding, there are two ways of imposing Dirichlet conditions: by Lagrange multiplier, or by restricting the space of admissible functions. The latter is not the same as the kind of explicit substitution you're doing here. If I take the functional defined in equation (15) and I *don't* separately impose the constraint $\boldsymbol{u} \cdot \boldsymbol{n} = 0$ at $\S_b$ on the arguments u_i, then I don;t see that taking the first variation of the functional will recover that constraint. If you impose the constraint $\boldsymbol{u} \cdot \boldsymbol{n} = 0$, then you do not need to make the substitution in equation (14) in the friction term of the Stokes Lagrangian

  The substitution here is again quite nonstandard, with little advance warning or real motivation. I think you're really trying to lay the groundwork for the modified Stokes variational principle later (by eliminating w where that's going to be necessary) but here is an awkward place to do it, unless you explain why you're eliminating w.

Again an oversight on my part! I should have pointed out that direct substitution is possible only in the discrete formulation of the functional where boundary variables are directly accessible (except of course in the surface integral terns where surface values are accessible even in the continuous formulation). I have tried to clarify this in the text.

- page 9 line 232 "...the specified values of velocity are then obtainable a posteriori from (9) or (14)" — this is a strange way of putting it. What is a specified value? One that is prescribed? I don't think that's what you mean. I think you mean that the taking the first variation does not recover the boundary condition $\boldsymbol{u} \cdot \boldsymbol{n} = 0$, see previous point. However, you can't impose that "a posteriori" since you cannot solve the Euler-Lagrange equations for the functional in (15) without using the Dirichlet condition on velocity. The standard way of putting this (I believe) is to restrict the functional to the vector space of suitable smooth velocities (in $[W^{1,1+1/n}(\Omega)]^3$) *that satisfy the Dirichlet condition.*

Yes, I do mean the prescribed values. I have changed the wording in the text to hopefully make this clearer.

- page 10, line 265 "The standard Stokes pressure P is some three orders of magnitude larger than the transformed pressure $\tilde{P}$" — asymptotic analysis of the problem will show that, more generally, the "Stokes correction" $\tilde{P}$ scales as $O(\varepsilon)$ when there is signfiicant sliding, where ε is aspect ratio, and of $O(\varepsilon^{1+1/n})$ in the absence of sliding (see the Schoof and Hindmarsh 2010 reference).

My main objective here was to highlight the absence of the large hydrostatic pressure component in the "Stokes correction".

- page 15 line 376 Remark # 1: seems like splitting hairs, especially as you wouldn't bother with this if you wrote down the weak form.

August 27, 2024

Maybe, but I think it's useful to point out that the presented BP equations differ, if only slightly, from the original.

- p 13 line 353 "The standard (or traditional) Blatter-Pattyn approximation (originally introduced by Blatter, 1995; Pattyn, 2003; later by DPL, 2010; Schoof and Hewitt, 2013)" — as above, Herterich (1987) was the person who introduced this. I don't think the Schoof and Hewitt review paper did much more than describe the theory, as oppposed to contributing to it. If I did anything here, then Schoof and Hindmarsh (2010) provided the first self-consistent asymptotic analysis of the model. If you want to list DPL for its description of the variatoinal formulation, you probably ought to cite the numerical analysis papers I have listed above (Coling and Rappaz, Glowinski and Rappaz, Chow et al, Rappaz and Reist; full citations in my 2010 paper that is in the reference list), who previously dealt with the same variational formulation.

Herterich is not pertinent since he did not introduce BP, just BP+. I've added "and references therein" to Schoof and Hewitt, 2013. Hope this is adequate. I'm reluctant to add a lot of extra references.

- page 15 line 419 "In summary, the extended Blatter-Pattyn model, (40)-(42), is equivalent to the standard Blatter-Pattyn model, (36), for the horizontal velocities, u,v , except that it also includes two additional equations that determine the pressure P ! and the vertical velocity w , which are usually ignored in the standard Blatter-Pattyn approximation when only the horizontal velocity is of interest. Because of this, we distinguish between the Blatter- Pattyn model that solves for just the two horizontal velocities (i.e., the standard Blatter- Pattyn approximation, (36)), and the Blatter-Pattyn system that solves for all the variables (i.e., the extended Blatter-Pattyn approximation, (40)-(42))." — again, this seems like splitting hairs. Anyone who needs to solve for temperature in an ice sheet (which is a standard part of any ice sheet simulation code) has to solve for the vertical velocity component, so I don't think insisting on a difference between the Blatter-Pattyn model and system is helpful. Solving for $\tilde{P}$ is not particularly relevant as we

  know $\tilde{P} = 0$ for the Blatter-Pattyn model. For the sake of not going down rabbit holes, I would omit this.

- p 17 line 437 "The use of the continuity equation to solve for the vertical velocity w is a novel feature of the Blatter-Pattyn approximation since the continuity equation is not normally used for this purpose." — as per my previous comment, I don't think this is true or novel. The vertical velocity component is a pretty important quantity to be able to compute in ice sheet codes.

- p 17 lie 439 onwards. The use of a depth-integrated mass conservation equation is a boilerplate approach for thin film models, so a lengthy discussion without citation seems unnecessary, especially as this doesn't really lead anywhere in developing the novel material in the paper.

I have rewritten the relevant sections and shortened them considerably. Hope this resolves the issue.

August 27, 2024

- p 17 line 482 "Additional details about the grid and the associated discretization..." — I flagged this above (grid versus mesh), but again: I think it's worth pointing out somewhere that some of the basis functions developed here really do require a regular mesh (grid?) rather than an unstructured triangulation. For the P1-E0 basis functions, I have to be able to match every triangle with precisely one neighbour, not leaving any neighbourless triangles. I don't think that's possible with every fully unstructured mesh. (?)

I think this is already done in Appendix B and especially in Fig. B2, which shows that the P1-E0 element is quite flexible and can be used with quite general triangulations. (Note: Appendix A has been eliminated so all remaining appendices have been renumbered.)

- page 19 line 504. Italicize the variables u and w.

Done

- page 21 line 526, "...or else they are "saddle point" problems since the Hessian matrix $M(u, w)$ is symmetric but indefinite, with both positive and negative eigenvalues..." — you can be more definitive about this I think: the "saddle point" terminology refers to the fact that there really is a saddle point, where you mimiize the quadratuc form associated with the matrix with respect to the velocity variables and maximize with respect to pressure.

I have added a sentence to this effect in the text.

- p 22 line 565 Please define the acronym "LBB" before using it.

Done on p. 22 in Section 4.3.1

- p 23 line 601 Taylor-Hood elements have gone from being an illustration of an element that satisfies the inf-sup condition (line 569) to becoming the standard reference for stable elements. Is it true in general that all elements that satisfy the LBB condition for the Stokes problem will leave M_{WP}^{T} non-invertible on dimensional grounds alone? If so, that is important to point out here.

Pointed out in Section 4.3.1

- Sections 5.1–5.3 You're focusing on velocity solutions here. If there are stability issues with your choice of basis functions, I'd expect these to show up in the pressure solution. Can we see resultss for some of those? Obviously not relevant for Herterich-Blatter-Pattyn, but for the transformed and original Stokes flow problems. Especially pressure along the bed would be useful, but also convergence or lack thereof.

I have added the following at the end of Section 5: "Pressure results are not shown because pressure, particularly in the transformed case, has little or no physical significance. However, pressure calculated on the P1-E0 grid is particularly smooth and well behaved."

August 27, 2024

- Figure 7: this is fine, but more convincing would be a grounding line, where you have to worry about a normal stress constraint determining the grounding line location (and that normal stress is in general not cryostatic as assumed by Herterich-Blatter-Pattyn)

That's true, but it's too late to make such a major change

Appendix - Identification of the Herterich model

From §3.4.1 of the present paper the 2D Blatter-Pattyn model is given by

$$\frac{\partial}{\partial x}\left(4\mu_{BP}\frac{\partial u}{\partial x}\right)+\frac{\partial}{\partial z}\left(\mu_{BP}\frac{\partial u}{\partial z}\right)-\rho g\frac{\partial z_s}{\partial x}=0\,, \tag{1}$$

where the effective viscosity is

$$\mu_{BP}=\eta_0\left(\dot{\varepsilon}_{BP}^2\right)^{(1-n)/2n}\,, \tag{2}$$

and the second invariant is

$$\dot{\varepsilon}_{BP}^2=\left(\frac{\partial u}{\partial x}\right)^2+\frac{1}{4}\frac{\partial u}{\partial z}^2\,. \tag{3}$$

After allowing for minor changes in notation, this is the same as found in Pattyn (2003), Schoof (2010), and DPL (2010).

The Herterich (1987) system, corresponding to (1)-(3), consists of his equations (2.11) and (2.12) which, using the present notation (i.e., x, u in the horizontal and z, w in the vertical), may be written as follows

$$\frac{\partial}{\partial x}\left(4\mu_H\frac{\partial u}{\partial x}\right)+\frac{\partial}{\partial z}\left(\mu_H\left(\frac{\partial u}{\partial z}+\frac{\partial w}{\partial x}\right)\right)-\rho g\frac{\partial z_s}{\partial x}=0,$$
$$\frac{\partial u}{\partial x}+\frac{\partial w}{\partial z}=0, \tag{4}$$

where

$$\mu_H=\frac{f}{2A^{1/n}}=\frac{1}{2A^{1/n}}\left(\dot{\varepsilon}_H^2\right)^{(1-n)/2n}\,, \tag{5}$$

and

$$\dot{\varepsilon}_H^2=\left(\frac{\partial u}{\partial x}\right)^2+\frac{1}{4}\left(\frac{\partial u}{\partial z}+\frac{\partial w}{\partial x}\right)^2\,. \tag{6}$$

Comparing (5) to (2), we can identify η_0 with $1/2A^{1/n}$. Thus, comparing Herterich's model, (4) and (5), to the Blatter-Pattyn model, (1)-(3), we see that the two models are

August 27, 2024

NOT the same because of the presence of the $\partial w / \partial x$ terms in the Herterich model.

(Note: There is a typo in Eq. (2.10) of the Herterich paper, i.e., $\partial v / \partial z$ should be $\partial v / \partial x$.)

Now, consider the BP+ approximation as given by the two functionals (62)-(64) from §6.2.1 in the paper. Ignoring the boundary condition terms since they don't matter for the present purpose, the functionals may be written as

$$\tilde{\mathcal{A}}_{PS1}[u] = \int_V dV \left[\frac{4n}{n+1} \eta_0 \left(\tilde{\dot{\varepsilon}}^2 \right)^{(1+n)/2n} + \rho g u \frac{\partial z_s}{\partial x} \right],$$

$$\tilde{\mathcal{A}}_{PS2}[p] = \int_V dV \ p \left(\frac{\partial u}{\partial x} + \frac{\partial w}{\partial z} \right),$$

(7)

where

$$\tilde{\dot{\varepsilon}}^2 = \left(\frac{\partial u}{\partial x} \right)^2 + \frac{1}{4} \left(\frac{\partial u}{\partial z} + \frac{\partial w}{\partial x} \right)^2.$$

(8)

Since $\eta_0 = 1/2 A^{1/n}$, the variation of $\tilde{\mathcal{A}}_{PS1}[u]$ with respect to u, and of $\tilde{\mathcal{A}}_{PS2}[p]$ with respect to p, yields precisely the Herterich system (4)-(6)! Together with the fact that $\tilde{\dot{\varepsilon}}^2 = \dot{\varepsilon}_H^2$, we conclude that Herterich's model is identically the same as the BP+ approximation.

A paragraph has been added to Section 6.2.1 pointing this out.

August 27, 2024

Changes in response to Prof. Bueler in Red.
Changes in response to Prof. Schoof in Blue.

1

A Novel Transformation of the Ice Sheet Stokes Equations and Some of its Properties and Applications

John K. Dukowicz

Guest Scientist, Group T-3, Los Alamos National Laboratory,

Los Alamos, New Mexico, 87545, USA

Correspondence to: John K. Dukowicz (jn.dk@outlook.com)

Abstract.   We introduce a novel transformation of the Stokes equations into a form that closely resembles the shallow Blatter-Pattyn equations. The two forms differ by only a few additional terms, while their variational formulations differ only by a single term in each horizontal direction. Specifically, the variational formulation of the Blatter-Pattyn model drops the vertical velocity in the second invariant of the strain rate tensor. Here we make use of the new transformation in two different ways. First, we consider incorporating the transformed equations into a code that can be very easily converted from a Stokes to a Blatter-Pattyn model, and vice-versa, by switching these terms on or off. This may be generalized so that the Stokes model is switched on adaptively only where the Blatter-Pattyn model loses accuracy. Second, the key role played by the vertical velocity in the Blatter-Pattyn approximation motivates new approximations that improve on the Blatter-Pattyn model. These applications require a grid that enables the discrete continuity equation to be invertible for the vertical velocity in terms of the horizontal velocity components. Examples of such grids, such as the first order P1-E0 grid and the second order P2-E1 grid are given in both 2D and 3D. It should be noted, however, that the transformed Stokes model has the same type of gravity forcing as the Blatter-Pattyn model, determined by the ice surface slope, thereby forgoing some of the grid-generality of the traditional formulation of the Stokes model.

1 Introduction

Concern and uncertainty about the magnitude of sea level rise due to melting of the Greenland and Antarctic ice sheets have led to increased interest in improved ice sheet and glacier modeling. The gold standard is a Stokes model (i.e., a model that solves the nonlinear, non-Newtonian Stokes system of equations for incompressible ice sheet dynamics) because it is applicable to all geometries and flow regimes. However, the Stokes model is computationally demanding and expensive to solve. It is a nonlinear, three-dimensional model involving four variables, namely, the three velocity components and pressure. In addition, pressure is a Lagrange multiplier enforcing incompressibility

August 30, 2024

38 and this creates a more difficult indefinite "saddle point" problem. As a result, full-

39 Stokes models exist but are not commonly used in practice (examples are FELIX-S, Leng

40 et al., 2012; Elmer/Ice, Gagliardini et al., 2013).

41

42 Because of these difficulties there is much interest in simpler and cheaper

43 approximate models. There is a hierarchy of very simple models such as the shallow ice

44 (SIA) and shallow-shelf (SSA) models, and there are also various more accurate higher-

45 order approximations. These culminate in the Blatter-Pattyn (BP) approximation

46 (Blatter, 1995; Pattyn, 2003), which is currently used in production code packages such

47 as ISSM (Larour et al., 2012), MALI (Hoffman et al., 2018; Tezaur et al., 2015) and

48 CISM (Lipscomb et al., 2019). This approximation is based on the assumption of a small

49 ice sheet aspect ratio, i.e., $\varepsilon = H/L \ll 1$, where H, L are the vertical and horizontal

50 length scales, and consequently it eliminates certain stress terms and implicitly assumes

51 small basal slopes. Both the Stokes and Blatter-Pattyn models are described in detail in

52 Dukowicz et al. (2010), hereafter referred to as DPL (2010). Although the Blatter-Pattyn

53 model is reasonably accurate for large-scale motions, accuracy deteriorates for small

54 horizontal scales, less than about five ice thicknesses in the ISMIP–HOM model

55 intercomparison (Pattyn et al., 2008; Perego et al., 2012), or below a 1 km resolution as

56 found in a detailed comparison with full Stokes calculations (Rückamp et al, 2022). This

57 can become particularly important for calculations involving details near the grounding

58 line where the full accuracy of the Stokes model is needed (Nowicki and Wingham,

59 2008). Attempts to address the problem while avoiding the use of full Stokes solvers

60 include variable grid resolution coupled with a Blatter-Pattyn solver (Hoffman et al.,

61 2018) and variable model complexity, where a Stokes solver is embedded locally in a

62 lower order model (Seroussi et al., 2012). Better approximations, more accurate than

63 Blatter-Pattyn but cheaper than Stokes, are currently not available.

64

65 The present paper introduces two innovations that may begin to address some of

66 these issues. The first is a novel transformation of the Stokes model, described in §3,

67 which puts it into a form closely resembling the Blatter-Pattyn model and differing only

68 by the presence of a few extra terms. This allows a code to be switched over from Stokes

69 to Blatter-Pattyn, and vice-versa, globally or locally, by the use of a single parameter that

70 turns off these extra terms. As a result, variable model complexity can be very simply

71 implemented, as described in §6.1. The second innovation is the introduction of new

August 30, 2024

72 finite element discretizations that decouple the discrete continuity equation and allow it to

73 be solved for the vertical velocity in terms of the horizontal velocity components.

74 Several elements used to construct such grids are described in Appendix C in both 2D

75 and 3D, primarily the first order P1-E0 and second order P2-E1 elements (these two

76 elements are novel and are so-named because they employ pressures located on vertical

77 grid edges). Within the framework of the transformed Stokes model these grids facilitate

78 new approximations that improve on the Blatter-Pattyn approximation so that it is no

79 longer strictly limited to a small ice sheet aspect ratio. We describe two such

80 approximations in §6.2. There is another very significant benefit. An ice sheet Stokes

81 model is conventionally discretized as a constrained minimization problem requiring

82 special "stable" finite elements for solution. However, the same model on these new

83 grids can be formulated as an inherently stable and numerically equivalent unconstrained

84 minimization problem, as demonstrated in §4.3.2.

85

86 **2 The Standard Formulation of the Stokes Ice Sheet Model**

87 **2.1 The Assumed Ice Sheet Configuration**

88

89 An ice sheet may be divided into two parts, a part in contact with the bed and a floating

90 ice shelf located beyond the grounding line. The Stokes ice sheet model is capable of

91 describing the flow of an arbitrarily shaped ice sheet, including a floating ice shelf as

92 illustrated in Fig. 1, given appropriate boundary conditions (e.g., Cheng et al., 2020).

93 One limitation of the methods proposed here, in common with the Blatter-Pattyn model,

94 will be that there should be just one upper and one basal surface, as is the case in Fig. 1.

95 Here we will only consider a fully grounded ice sheet with periodic lateral boundary

96 conditions, i.e., no ice shelf, although in general ice shelves can be handled.
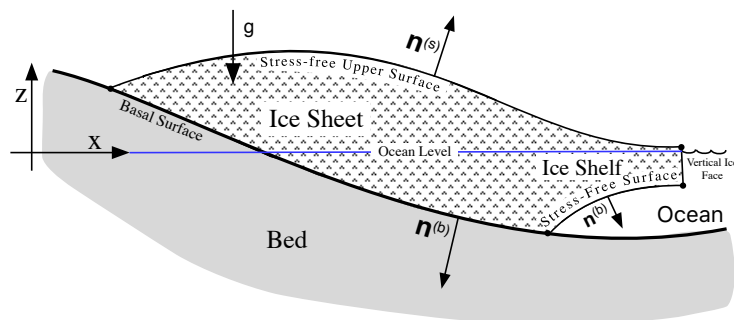
97
98
99 **Figure 1** A simplified illustration of the admissible ice sheet configuration.
100

August 30, 2024

101

102   Referring to Fig. 1, the entire surface of the ice sheet is denoted by S. An upper

103 surface, labeled S_s and specified by $\varsigma_s(x,y,z)=z-z_s(x,y)=0$, is exposed to the

104 atmosphere and thus experiences stress-free boundary conditions. The bottom or basal

105 surface, denoted by S_B and specified by $\varsigma_b(x,y,z)=z-z_b(x,y)=0$, is in contact with

106 the bed. The basal surface may be subdivided into two sections, $S_B = S_{B1} \cup S_{B2}$, where

107 S_{B1}, specified by $z=z_{b1}(x,y)$, is the part where ice is frozen to the bed (a no-slip

108 boundary condition), and S_{B2}, specified by $z=z_{b2}(x,y)$, is where frictional sliding

109 occurs. We assume Cartesian coordinates such that $x_i = (x,y,z)$ are position coordinates

110 with $z=0$ at the ocean surface, and the index $i \in \{x,y,z\}$ represents the three Cartesian

111 indices. Later we shall have occasion to introduce the restricted index $(i) \in \{x,y\}$ to

112 represent just the two horizontal indices. Note that this is equivalent to applying a

113 projection operator but is more compact, i.e., $u_{(i)} = P_i(u) = (u,v,0)$. Unit normal vectors

114 appropriate for the ice sheet configuration of Fig. 1 are given by

115
$$n_i = (n_x, n_y, n_z) = \frac{\partial \varsigma_s(x,y,z)/\partial x_i}{\left|\partial \varsigma_s(x,y,z)/\partial x_i\right|} = \frac{(-\partial z_s/\partial x, -\partial z_s/\partial y, 1)}{\sqrt{1+(\partial z_s/\partial x)^2+(\partial z_s/\partial y)^2}} \qquad \text{at surface } S_s,$$

$$n_i = (n_x, n_y, n_z) = -\frac{\partial \varsigma_b(x,y,z)/\partial x_i}{\left|\partial \varsigma_b(x,y,z)/\partial x_i\right|} = \frac{(\partial z_b/\partial x, \partial z_b/\partial y, -1)}{\sqrt{1+(\partial z_b/\partial x)^2+(\partial z_b/\partial y)^2}} \qquad \text{at surface } S_B.$$
(1)

116

117 **2.2 The Stokes Equations**

118

119 The Stokes model is a system of nonlinear partial differential equations and associated

120 boundary conditions (Greve and Blatter, 2009; DPL, 2010). In a Cartesian coordinate

121 system the Stokes equations, the three momentum equations and the continuity equation,

122 for the three velocity components $u_i = (u,v,w)$ and the pressure P are given by

123
$$\frac{\partial \tau_{ij}}{\partial x_j} - \frac{\partial P}{\partial x_i} + \rho g_i = 0 \;,$$
(2)

August 30, 2024

124
$$\frac{\partial u_i}{\partial x_i} = 0 \, , \tag{3}$$

125 where ρ is the density, and g_i is the acceleration vector due to gravity, arbitrarily

126 oriented in general but here taken to be in the negative z-direction, $g_i = (0,0,-g)$.

127 Repeated indices imply summation (the Einstein notation). The deviatoric stress tensor

128 τ_{ij} is given by

129
$$\tau_{ij} = 2\mu_n \, \dot{\varepsilon}_{ij} \, , \tag{4}$$

130 where the strain rate tensor is

131
$$\dot{\varepsilon}_{ij} = \frac{1}{2}\left(\frac{\partial u_i}{\partial x_j} + \frac{\partial u_j}{\partial x_i} \right) , \tag{5}$$

132 the nonlinear ice viscosity μ_n is a defined by

133
$$\mu_n = \eta_0 \left(\dot{\varepsilon}^2 \right)^{(1-n)/2n} \, , \tag{6}$$

134 and $\dot{\varepsilon}^2 = \dot{\varepsilon}_{ij}\dot{\varepsilon}_{ij}/2$ is the second invariant of the strain rate tensor that may be written out

135 in full as follows

136
$$\dot{\varepsilon}^2 = \frac{1}{2}\left[\left(\frac{\partial u}{\partial x}\right)^2 + \left(\frac{\partial v}{\partial y}\right)^2 + \left(\frac{\partial w}{\partial z}\right)^2 \right] + \frac{1}{4}\left[\left(\frac{\partial u}{\partial y}+\frac{\partial v}{\partial x}\right)^2 + \left(\frac{\partial u}{\partial z}+\frac{\partial w}{\partial x}\right)^2 + \left(\frac{\partial v}{\partial z}+\frac{\partial w}{\partial y}\right)^2 \right]. \tag{7}$$

137 Note that the second invariant is a positive quantity, i.e., $\dot{\varepsilon}^2 \geq 0$. As usual, ice is assumed

138 to obey Glen's flow law, where n is the Glen's law exponent ($n=1$ for a linear

139 Newtonian fluid. Typically $n=3$ in ice sheet modeling, resulting in a nonlinear non-

140 Newtonian fluid). The coefficient η_0 is defined by $\eta_0 = A^{-1/n}/2$, where A is an ice flow

141 factor, here taken to be a constant but in general depending on temperature and other

142 variables (see Schoof and Hewitt, 2013). The three-dimensional Stokes system requires a

143 set of boundary conditions at every bounding surface, each set being composed of three

144 components. Aside from the periodic lateral boundary conditions used in our test

145 problems, the relevant boundary conditions are given as follows

146   (1) Stress-free boundary conditions on surfaces S_S not in contact with the bed, such

147 as the upper surface S_S:

148
$$\tau_{ij}n_j - Pn_t = 0 \, . \tag{8}$$

August 30, 2024

149   (2) No-slip or frozen to the bed conditions on surface segment S_{B1}:

150
$$u_i = 0 \tag{9}$$

151   (3) Frictional tangential sliding conditions on surface segment S_{B2} in two parts:

152   (3a) A single condition enforcing tangential flow at the basal surface:

153
$$u_i n_i = 0 \,. \tag{10}$$

154   (3b) Two conditions specifying the horizontal components of the tangential

155 frictional stress force vector, as follows

156
$$\tau_{(i)j} n_j - \tau_n n_{(i)} + \tau_{(i)}^S = 0 \,, \tag{11}$$

157 where $\tau_n = n_i \tau_{ij} n_j$ is the normal component of the shear stress, and τ_i^S is a specified

158 interfacial shear stress, tangential to the bed $\left(n_i \tau_i^S = 0 \right)$. The tangential shear stress or

159 traction is obtained as in DPL (2010) by subtracting out the normal component from the

160 shear stress. However, the three components of the tangential shear stress are not

161 independent because they already satisfy the tangency condition at the basal surface and

162 therefore we retain only the horizontal components. The interfacial shear stress τ_i^S is

163 potentially a complicated function of position and velocity (e.g., Schoof, 2010).

164 However, here we assume only simple linear frictional sliding,

165
$$\tau_i^S = \beta(x) u_i \,, \tag{12}$$

166 where $\beta(x) > 0$ is a position-dependent drag law coefficient. For simplicity we assume

167 there is no melting or refreezing at the bed resulting in vertical inflows or outflows. If

168 needed, these can be easily added to (10) (Dukowicz et al., 2010; Heinlein et al., 2022).

169

170 **2.3 The Stokes Variational Principle**

171

172 A variational principle, if available, is usually the most compact way of representing a

173 particular problem. The Stokes model possesses a variational principle that is

174 particularly useful for discretization purposes and for the specification of boundary

175 conditions (see DPL, 2010, and Chen et al., 2013, for a fuller description of the

176 variational principle applied to ice sheet modeling). There are a number of significant

177 advantages. For example, all boundary conditions are conveniently incorporated in the

178 variational formulation, all terms in the variational functional, including boundary

179 condition terms, contain lower order derivatives than in the momentum equations, and the

August 30, 2024

180   resulting discretization automatically involves a symmetric matrix. In discretizing the

181   momentum equations, stress terms at boundaries involve derivatives that would normally

182   have to be evaluated using less accurate one-sided approximations. This problem does

183   not arise in the variational formulation since all terms are evaluated in the interior.

184   Finally, stress-free boundary conditions, as at the upper surface for example, need not be

185   specified at all since they are automatically incorporated in the functional as natural

186   boundary conditions. In discrete applications, the variational method presented here is

187   closely related to the Galerkin finite element method, a subset of the weak formulation

188   method in which the test and trial functions are the same (see Schoof, 2010, and earlier

189   references contained therein in connection with the Blatter-Pattyn model).

190

191   The variational functional for the standard Stokes model may be written in two

192   alternative forms:

193   (1) Basal boundary conditions imposed using Lagrange multipliers:

$$
\mathcal{A}[u_i, P, \lambda_i, \Lambda] = \int_V dV \left[\frac{4n}{n+1} \eta_0 \left(\dot{\varepsilon}^2 \right)^{(1+n)/2n} - P \frac{\partial u_i}{\partial x_i} + \rho g w \right]
$$

194   (13)

$$
+ \int_{S_{B1}} dS\, \lambda_i u_i + \int_{S_{B2}} dS \left[\Lambda u_i n_i + \frac{1}{2} \beta(x)\, u_i u_i \right],
$$

195   where λ_i and Λ are Lagrange multipliers used to enforce the no-slip condition and

196   frictional tangential sliding, respectively. As in DPL (2010), arguments enclosed in

197   square brackets, here $u_i, P, \lambda_i, \Lambda$, indicates those functions that are subject to variation as

198   arguments of the functional.

199   (2) Basal boundary conditions imposed by direct substitution:

200   In this case, the two conditions (9), (10) are used directly in the functional to specify all

201   three velocity components u_i in the first case, and the vertical velocity w in terms of the

202   horizontal velocity components in the second case, along the entire basal boundary in

203   both the volume and surface integrals in (13). However, this can only be done in the

204   discrete formulation of the functional since only then are boundary values of velocity

205   accessible (except in the surface integral terms where they are always accessible). In

206   particular, the tangential flow condition (10) is used in the following form,

$$
w = -\frac{u_{(i)} n_{(i)}}{n_z} = u_{(i)} \frac{\partial z_b}{\partial x_{(i)}},
$$

207   (14)

208   to eliminate w on the basal boundary segment S_{B2} of the variational functional, to obtain

$$\mathcal{A}[u_i, P] = \int_V dV \left[\frac{4n}{n+1} \eta_0 \left(\dot{\varepsilon}^2 \right)^{(1+n)/2n} - P \frac{\partial u_i}{\partial x_i} + \rho g w \right]$$
$$+ \frac{1}{2} \int_{S_{B2}} dS \, \beta(x) \left(u_{(i)} u_{(i)} + \left(u_{(i)} n_{(i)} \big/ n_z^{(b2)} \right)^2 \right).$$

(15)

209

210   It is important to emphasize again that boundary conditions (9) and (14) must also be
211   applied in the volume integral part of the discretized functional (15) as part of direct
212   substitution to replace velocity variables that lie on the basal boundary. In the case of
213   (14), horizontal velocity variables remain undisturbed while w is eliminated, thus
214   implementing the tangential sliding boundary condition.
215

216   As described in DPL (2010), a variational procedure yields the full set of Euler-
217   Lagrange equations and boundary conditions that specify the standard Stokes model,
218   equivalent to (2)-(11). In the case of (13), the system determines all the discrete variables
219   specified on the mesh: the velocity components and the pressure, u_i, P, as well as the
220   Lagrange multipliers, λ_i, Λ. In the direct substitution case, (15), the numerical solution
221   determines only the pressure P and those velocity variables u_i that were not directly
222   prescribed as boundary conditions in (9) or (14). These prescribed (known) values of
223   boundary velocities are then added a posteriori. As a result, the direct substitution
224   method is smaller and simpler, and therefore is the one primarily used in the paper.
225

226   **3. A Transformation of the Stokes Model**
227   **3.1 Origin of the Transformation**
228

229   The transformation is motivated by the Blatter-Pattyn approximation. Consider the
230   vertical component of the momentum equation and the corresponding stress-free upper
231   surface boundary condition in the Blatter-Pattyn approximation (from DPL, 2010, for
232   example), which are given by

$$\frac{\partial}{\partial z} \left(2\mu_n \frac{\partial w}{\partial z} \right) - \frac{\partial P}{\partial z} - \rho g = 0,$$

233

$$\left(2\mu_n \frac{\partial w}{\partial z} - P \right) n_z = 0 \quad \text{at} \quad z = z_s(x, y).$$

(16)

234   These equations may be rewritten in the form

August 30, 2024

$$\frac{\partial}{\partial z}\left(P - 2\mu_n \frac{\partial w}{\partial z} + \rho g\left(z - z_s(x,y)\right)\right) = 0,$$

$$\left(P - 2\mu_n \frac{\partial w}{\partial z} + \rho g\left(z - z_s(x,y)\right)\right)n_z = 0 \quad \text{at} \quad z = z_s(x,y), \tag{17}$$

236 suggesting a new variable $\tilde{P}$, to be called the transformed pressure, as follows

$$\tilde{P} = P - 2\mu_n \frac{\partial w}{\partial z} + \rho g\left(z - z_s(x,y)\right), \tag{18}$$

238 which simplifies system (17) to give

$$\frac{\partial \tilde{P}}{\partial z} = 0,$$

$$\tilde{P}n_z = 0 \quad \text{at} \quad z = z_s(x,y). \tag{19}$$

240 This is a complete one-dimensional partial differential system, that, when integrated from
241 the top surface down yields

$$\tilde{P} = 0. \tag{20}$$

243 Thus, the transformed pressure vanishes in the Blatter-Pattyn case. The definition (18)
244 forms the basis of the present transformation but we also use the continuity equation to

245 eliminate $\partial w/\partial z$ as is done in the Blatter-Pattyn approximation (e.g., Pattyn, 2003).

246 Therefore, the transformation consists of eliminating P and $\partial w/\partial z$ in the Stokes system
247 (2), (4)-(11) (i.e., everywhere except in the continuity equation (3) itself) by means of

$$P = \tilde{P} - 2\mu_n\left(\frac{\partial u}{\partial x} + \frac{\partial v}{\partial y}\right) + \rho g\left(z_s - z\right), \tag{21}$$

$$\frac{\partial w}{\partial z} = -\left(\frac{\partial u}{\partial x} + \frac{\partial v}{\partial y}\right). \tag{22}$$

250

251 The pressure P in the standard Stokes system is primarily a Lagrange multiplier
252 enforcing incompressibility, but with a very large hydrostatic component. The
253 transformation eliminates the hydrostatic pressure from $\tilde{P}$, as illustrated in Fig. 2 where
254 the two pressures are compared. The transformed pressure $\tilde{P}$ is some three orders of
255 magnitude smaller than the standard Stokes pressure P primarily because of the absence
256 of hydrostatic pressure.

August 30, 2024
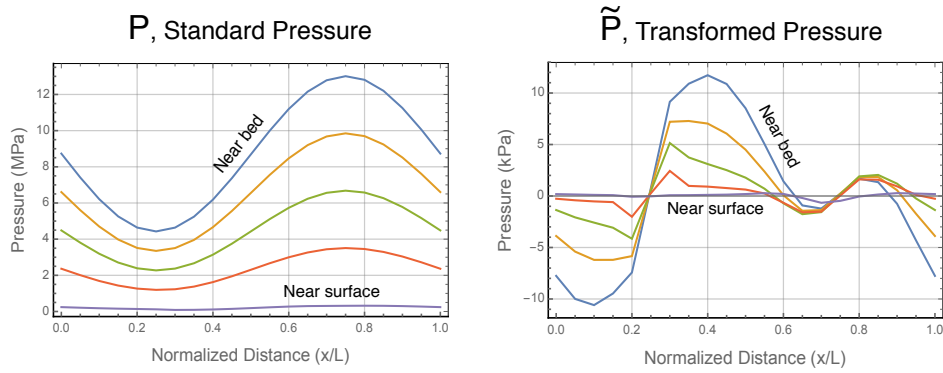
Figure 2. Standard pressure P compared to the transformed pressure $\tilde{P}$ in Exp. B from the ISMIP–HOM model intercomparison (Pattyn et al., 2008) at L = 10 km. Note that P is in MPa while $\tilde{P}$ is in kPa.

The transformed pressure $\tilde{P}$ is again a Lagrange multiplier enforcing incompressibility. Alternatively, since $\tilde{P} = 0$ in the Blatter-Pattyn approximation, the transformed pressure may be written as $\tilde{P} = P - P_{BP}$, where

$$P_{BP} = -2\mu_n \left(\frac{\partial u}{\partial x} + \frac{\partial v}{\partial y} \right) + \rho g \left(z_s - z \right)$$

is the effective Blatter-Pattyn pressure (Tezaur et al., 2015). As a result, $P = P_{BP} + \tilde{P}$ and therefore $\tilde{P}$ is actually the "Stokes" correction to the Blatter-Pattyn pressure.

3.2 The Transformed Stokes Equations

Introducing (21), (22) into the Stokes system of equations (2)-(11) results in the following transformed Stokes system:

$$\frac{\partial \tilde{\tau}_{ij}}{\partial x_j} - \hat{\xi} \frac{\partial \tilde{P}}{\partial x_i} - \rho g \frac{\partial z_s}{\partial x_{(i)}} = 0 , \tag{23}$$

$$\hat{\xi} \frac{\partial u_i}{\partial x_i} = 0 , \tag{24}$$

where quantities that are modified in the transformation are indicated by a tilde, e.g., $\tilde{P}$.

Here and in the following we will be using dummy variables $\xi, \hat{\xi}$ to indicate terms that

August 30, 2024

277 are absent in the Blatter-Blatter approximation, as explained below. Corresponding to (4)

278 the modified Stokes deviatoric stress tensor $\tilde{\tau}_{ij}$ is given by

$$\tilde{\tau}_{ij} = 2\tilde{\mu}_n\left(\tilde{\dot{\varepsilon}}_{ij} + \frac{\partial u_{(i)}}{\partial x_{(i)}}\delta_{ij} \right), \tag{25}$$

280 where δ_{ij} is the Kronecker delta, the modified strain rate tensor $\tilde{\dot{\varepsilon}}_{ij}$, corresponding to (5),

281 is given by

$$\tilde{\dot{\varepsilon}}_{ij} = \begin{bmatrix} \dfrac{\partial u}{\partial x} & \dfrac{1}{2}\left(\dfrac{\partial u}{\partial y}+\dfrac{\partial v}{\partial x}\right) & \dfrac{1}{2}\left(\dfrac{\partial u}{\partial z}+\xi\dfrac{\partial w}{\partial x}\right) \\[2mm] \dfrac{1}{2}\left(\dfrac{\partial u}{\partial y}+\dfrac{\partial v}{\partial x}\right) & \dfrac{\partial v}{\partial y} & \dfrac{1}{2}\left(\dfrac{\partial v}{\partial z}+\xi\dfrac{\partial w}{\partial y}\right) \\[2mm] \dfrac{1}{2}\left(\dfrac{\partial u}{\partial z}+\xi\dfrac{\partial w}{\partial x}\right) & \dfrac{1}{2}\left(\dfrac{\partial v}{\partial z}+\xi\dfrac{\partial w}{\partial y}\right) & -\left(\dfrac{\partial u}{\partial x}+\dfrac{\partial v}{\partial y}\right) \end{bmatrix} \tag{26}$$

283 and, corresponding to (6), the modified viscosity,

$$\tilde{\mu}_n = \eta_0\left(\tilde{\dot{\varepsilon}}^2\right)^{(1-n)/2n}, \tag{27}$$

285 is given in terms of the second invariant, $\tilde{\dot{\varepsilon}}^2 = \tilde{\dot{\varepsilon}}_{ij}\tilde{\dot{\varepsilon}}_{ij}/2$, that in expanded form becomes

$$\tilde{\dot{\varepsilon}}^2 = \left(\frac{\partial u}{\partial x}\right)^2 + \frac{\partial u}{\partial x}\frac{\partial v}{\partial y} + \left(\frac{\partial v}{\partial y}\right)^2 + \frac{1}{4}\left[\left(\frac{\partial u}{\partial y}+\frac{\partial v}{\partial x}\right)^2 + \left(\frac{\partial u}{\partial z}+\xi\frac{\partial w}{\partial x}\right)^2 + \left(\frac{\partial v}{\partial z}+\xi\frac{\partial w}{\partial y}\right)^2\right]. \tag{28}$$

287 Since (28) differs from (7) only by the use of the continuity equation (22), the

288 transformation will leave the second invariant $\tilde{\dot{\varepsilon}}^2$ and viscosity $\tilde{\mu}_n$ unchanged, i.e.,

289 $\tilde{\dot{\varepsilon}}^2 = \dot{\varepsilon}^2$ and $\tilde{\mu}_n = \mu_n$, and the transformed second invariant remains positive, i.e., $\tilde{\dot{\varepsilon}}^2 \geq 0$.

290

291   The dummy variables $\xi, \hat{\xi}$ in (23)-(25) and (26)-(29) are used to identify terms

292 that are neglected in the two types of the Blatter-Pattyn approximation discussed in §3.4.

293 These are (a) the standard Blatter-Pattyn approximation, $\xi = 0, \hat{\xi} = 0$, as originally

294 derived (Blatter, 1995; Pattyn, 2003; DPL, 2010), which solves for just the horizontal

295 velocity components u, v, and (b) the extended Blatter-Pattyn approximation,

296 $\xi = 0, \hat{\xi} = 1$, described more fully later, that contains the standard approximation and also

August 30, 2024

297   contains additional equations that determine the vertical velocity w and the pressure $\tilde{P}$.

298   Keeping all terms, i.e., $\xi = 1, \hat{\xi} = 1$, specifies the full transformed Stokes model.

299

300   Boundary conditions for the transformed equations, corresponding to (8)-(11), are

301   given by

302   BCs on S_S:
$$\tilde{\tau}_{ij} n_j - \hat{\xi} \tilde{P} n_i = 0 , \tag{29}$$

303   BCs on S_{B1}:
$$u_i = 0 , \tag{30}$$

304   BCs on S_{B2}:
$$u_i n_i = 0 , \tag{31}$$

305
$$\tilde{\tau}_{(i)j} n_j - \tilde{\tau}_n n_{(i)} + \beta(x) u_{(i)} = 0 , \tag{32}$$

306   where $\tilde{\tau}_n = n_i \tilde{\tau}_{ij} n_j$ as before. Equations (31), (32) constitute the three required boundary

307   conditions for frictional sliding.

308

309   The transformed system, (25)-(32), and the standard Stokes system, (2)-(11), yield

310   exactly the same solution. However, in common with the Blatter-Pattyn approximation,

311   transformation (21) needs to use a gravity-oriented coordinate system because of the

312   particular form of the gravitational forcing term, while the standard Stokes model does

313   not have this restriction. This is not a major limitation. A somewhat more restrictive

314   limitation is the appearance of $z_s(x,y)$, an implicitly single valued function, to describe

315   the vertical position of the upper surface of the ice sheet. This means that care must be

316   taken in case of reentrant upper surfaces (i.e., S-shaped in 2D) and sloping cliffs at the ice

317   edge, a restriction not present in the standard Stokes model. For simplicity, as noted

318   before we assume that there is just one upper and one basal surface, i.e., as is usual in ice

319   sheet modeling we do not permit overhangs.

320

321   **3.3 The Transformed Stokes Variational Principle**

322

323   It is easy to verify that the transformed Stokes system (23)-(32) results from the variation

324   with respect to $u_i, \tilde{P}$ of the following functional:

August 30, 2024

$$\tilde{\mathcal{A}}[u_i, \tilde{P}] = \int_V dV \left[\frac{4n}{n+1} \eta_0 \left(\tilde{\varepsilon}^2 \right)^{(1+n)/2n} - \hat{\xi} \tilde{P} \frac{\partial u_i}{\partial x_i} + \rho g u_{(i)} \frac{\partial z_s}{\partial x_{(i)}} \right]$$
$$+ \frac{1}{2} \int_{S_{B2}} dS\, \beta(x) \left(u_{(i)} u_{(i)} + \left(u_{(i)} n_{(i)} / n_z \right)^2 \right), \tag{33}$$

where $\tilde{\varepsilon}^2$ is the transformed second invariant from (28). Basal boundary conditions are imposed by direct substitution, as in (15). Alternatively, one could also impose boundary conditions using Lagrange multipliers as in (13), if desired.

3.4 Two Blatter-Pattyn Approximations
3.4.1 The Standard Blatter-Pattyn Approximation

The standard (or traditional) Blatter-Pattyn approximation (originally introduced by Blatter, 1995; Pattyn, 2003; later by DPL, 2010; Schoof and Hewitt, 2013, and references therein) is obtained by setting $\xi = 0, \hat{\xi} = 0$ in the transformed system. This yields the following Blatter-Pattyn variational functional,

$$\mathcal{A}_{BP}[u_{(i)}] = \int_V dV \left[\frac{4n}{n+1} \eta_0 \left(\dot{\varepsilon}_{BP}^2 \right)^{(1+n)/2n} + \rho g u_{(i)} \frac{\partial z_s}{\partial x_{(i)}} \right]$$
$$+ \frac{1}{2} \int_{S_{B2}} dS\, \beta(x) \left(u_{(i)} u_{(i)} + \varsigma \left(u_{(i)} n_{(i)} / n_z \right)^2 \right), \tag{34}$$

in terms of horizontal velocity components only, where the second invariant $\dot{\varepsilon}_{BP}^2$ follows from (28) with $\xi = 0$,

$$\dot{\varepsilon}_{BP}^2 = \left(\frac{\partial u}{\partial x} \right)^2 + \frac{\partial u}{\partial x} \frac{\partial v}{\partial y} + \left(\frac{\partial v}{\partial y} \right)^2 + \frac{1}{4} \left[\left(\frac{\partial u}{\partial y} + \frac{\partial v}{\partial x} \right)^2 + \frac{\partial u}{\partial z}^2 + \frac{\partial v}{\partial z}^2 \right], \tag{35}$$

and therefore the Euler-Lagrange equations and boundary conditions become

$$\frac{\partial \tau_{(i)j}^{BP}}{\partial x_j} - \rho g \frac{\partial z_s}{\partial x_{(i)}} = 0; \quad \begin{cases} \tau_{(i)j}^{BP} n_j + \beta(x) \left(u_{(i)} + \zeta \left(u_{(j)} n_{(j)} / n_z \right) n_{(i)} / n_z \right) = 0 \\ \text{on } S_{B2}, \quad \tau_{(i)j}^{BP} n_j = 0 \text{ on } S_S, \quad u_{(i)} = 0 \text{ on } S_{B1}, \end{cases} \tag{36}$$

where the Blatter-Pattyn stress tensor $\tau_{(i)j}^{BP}$ is

$$\tau_{(i)j}^{BP} = \eta_0 \left(\dot{\varepsilon}_{BP}^2\right)^{(1-n)/2n} \begin{bmatrix} 2\left(2\dfrac{\partial u}{\partial x} + \dfrac{\partial v}{\partial y}\right) & \left(\dfrac{\partial u}{\partial y} + \dfrac{\partial v}{\partial x}\right) & \dfrac{\partial u}{\partial z} \\[2mm] \left(\dfrac{\partial u}{\partial y} + \dfrac{\partial v}{\partial x}\right) & 2\left(\dfrac{\partial u}{\partial x} + 2\dfrac{\partial v}{\partial y}\right) & \dfrac{\partial v}{\partial z} \end{bmatrix}. \tag{37}$$

These last two equations correspond to (23) and (25) in the transformed Stokes system.

There is a new dummy variable ζ in (34) introduced to identify the basal boundary term

normally dropped $(\zeta = 0)$ in the standard Blatter-Pattyn approximation but restored

$(\zeta = 1)$ in Dukowicz et al. (2011) to better deal with arbitrary basal topography.

     The Blatter-Pattyn model is a well-behaved nonlinear approximate system for the
horizontal velocity components u, v because in this case the variational formulation is a
convex optimization problem whose solution minimizes the functional. As noted in the
Introduction, the Blatter-Pattyn approximation is widely used in practice as an
economical and relatively accurate ice sheet model. If desired, the vertical velocity
component w may be computed a posteriori by means of the continuity equation.

Remark #1: The original formulation (e.g., Pattyn, 2003) approximates the normal unit

vectors n_i on the frictional part of the basal boundary S_{B2} by making the small slope

approximation. However, this additional approximation is unnecessary since any
computational savings are negligible (Dukowicz et al., 2011; Perego et al., 2012).

3.4.2 The Extended Blatter-Pattyn Approximation

A second form of the Blatter-Pattyn approximation is obtained from the transformed
variational principle (33) by making the assumption,

$$\left\|\frac{\partial w}{\partial x}\right\| \ll \left\|\frac{\partial u}{\partial z}\right\|, \quad \left\|\frac{\partial w}{\partial y}\right\| \ll \left\|\frac{\partial v}{\partial z}\right\|, \tag{38}$$

and therefore neglecting $\partial w/\partial x, \partial w/\partial y$ in the transformed second invariant $\tilde{\varepsilon}^2$, or

equivalently, in the strain rate tensor $\tilde{\varepsilon}_{ij}$ from (26), consistent with the original small

aspect ratio approximation (Blatter, 1995; Pattyn, 2003; DPL, 2010; Schoof and

Hindmarsh, 2008). This corresponds to setting $\xi = 0, \hat{\xi} = 1$ in the transformed Stokes

model. In other words, we neglect vertical velocity gradients but keep the pressure term.

372   This will be called the extended Blatter-Pattyn approximation (EBP) because, in contrast

373   to the standard Blatter-Pattyn approximation, all the variables, i.e., $u, v, w, \tilde{P}$, are retained.

374   Notably, assumption (38) is equivalent to just setting $w = 0$ in the second invariant $\tilde{\dot{\varepsilon}}^2$ in

375   the full transformed Stokes model. That is, the extended BP approximation is obtained

376   by neglecting vertical velocities everywhere in (33) except where they occurs in the

377   velocity divergence term. This aspect of the transformed Stokes model will be exploited

378   later to obtain approximations that improve on Blatter-Pattyn. Thus, the extended

379   Blatter-Pattyn functional is given by

380

$$
\mathcal{A}_{EBP}[u_i, \tilde{P}] = \int_V dV \left[\frac{4n}{n+1} \eta_0 \left(\dot{\varepsilon}_{BP}^2 \right)^{(1+n)/2n} - \tilde{P} \frac{\partial u_i}{\partial x_i} + \rho g u_{(i)} \frac{\partial z_s}{\partial x_{(i)}} \right]
$$
$$
+ \frac{1}{2} \int_{S_{B2}} dS \, \beta(x) \left(u_{(i)} u_{(i)} + \varsigma \left(u_{(i)} n_{(i)} / n_z \right)^2 \right),
$$
(39)

381   and the Blatter-Pattyn second invariant $\dot{\varepsilon}_{BP}^2$ is given by (35). Taking the variation of the

382   functional, the system of extended Blatter-Pattyn Euler-Lagrange equations and their

383   boundary conditions is given by

384   (1) Variation with respect to $u_{(i)}$ yields the horizontal momentum equation:

385

$$
\frac{\partial \tau_{(i)j}^{BP}}{\partial x_j} - \frac{\partial \tilde{P}}{\partial x_{(i)}} - \rho g \frac{\partial z_s}{\partial x_{(i)}} = 0; \quad
\begin{cases}
\tau_{(i)j}^{BP} n_j - \tilde{P} n_{(i)} = 0 \text{ on } S_S, \quad u_{(i)} = 0 \text{ on } S_{B1}, \\
\tau_{(i)j}^{BP} n_j + \beta(x) \left(u_{(i)} + \zeta \left(u_{(k)} n_{(k)} / n_z \right) n_{(i)} / n_z \right) = 0 \\
\qquad\qquad \text{on } S_{B2},
\end{cases}
$$
(40)

386   where $\tau_{(i)j}^{BP}$ is given by (37).

        (2) Variation with respect to w yields the vertical momentum equation:

388

$$
-\frac{\partial \tilde{P}}{\partial z} = 0; \qquad \tilde{P} n_z = 0 \text{ on } S_S,
$$
(41)

389   (3) Variation with respect to $\tilde{P}$ yields the continuity equation:

390

$$
\frac{\partial w}{\partial z} + \frac{\partial u_{(i)}}{\partial x_{(i)}} = 0; \quad w = 0 \text{ on } S_{B1}, \text{ or } w = -u_{(i)} n_{(i)} / n_z \text{ on } S_{B2}.
$$
(42)

391   It is apparent that the vertical momentum equation system (41) is decoupled, yielding

392    $\tilde{P} = 0$, as was already shown in §3.1. This eliminates pressure from the horizontal

393   momentum equation (40), making it a decoupled equation for the horizontal velocities

August 30, 2024

394 $u_{(i)}$, identical to the standard Blatter-Pattyn system (36). In addition, having obtained the

395 horizontal velocities from (40), the continuity equation (42) may now be solved for the

396 vertical velocity w (but see the comments regarding the discrete case that follow (43)).

397

398 In summary, the extended Blatter-Pattyn model, (40)-(42), is equivalent to the

399 standard Blatter-Pattyn model, (36), for the horizontal velocities, u, v, except that it also

400 includes two additional equations that determine the pressure $\tilde{P}$ and the vertical velocity

401 w that are usually ignored in the standard Blatter-Pattyn approximation where only the

402 horizontal velocity is calculated. Because of this, we distinguish between the _Blatter-_

403 _Pattyn model_ that solves for just the two horizontal velocities (i.e., the standard Blatter-

404 Pattyn approximation, (36)), and the _Blatter-Pattyn system_ that solves for all the variables

405 (i.e., the extended Blatter-Pattyn approximation, (40)-(42)). Perhaps the main distinction

406 between the two, which may be imporant in some applications, is that the Blatter-Pattyn

407 system obtains the vertical velocity on the same grid as the horizontal velocities, while in

408 the Blatter-Pattyn model the calculation of vertical velocity is completely decoupled and

409 may be done on an unrelated grid. These models must obtain the vertical velocity w

410 from the continuity equation (42) once horizontal velocities u, v are available. In the

411 continuous case this can be done using the Leibniz's theorem, as follows

412 $$w(u,v) = w_{z=z_b} - \int_{z_b}^{z} \frac{\partial u_{(i)}}{\partial x_{(i)}} dz' = u_{(i)} \frac{\partial z_b}{\partial x_{(i)}} - \int_{z_b}^{z} \frac{\partial u_{(i)}}{\partial x_{(i)}} dz' = -\frac{\partial}{\partial x_{(i)}} \int_{z_b}^{z} u_{(i)} dz'. \qquad (43)$$

413 In the discrete case one may consider discretizing (43) directly. However, later we

414 consider special finite element grids where the continuity equation is stably solved for w.

415

416 So far we have only considered continuum properties of Stokes-type systems.

417 However, a discrete finite element formulation may not be well behaved. The solution of

418 discretized Stokes models and Blatter-Pattyn approximations, and the solution for vertical

419 velocity from the continuity equation will depend on the choices made for the grids and

420 the finite elements that are to be used. These issues will be discussed next.

421

422 **4. Finite Element Discretization**

423 **4.1 Standard and Transformed Stokes Discretizations**

424

425 In practice, both traditional Stokes and Blatter-Pattyn models are discretized using finite

426 element methods (e.g., Gagliardini et al., 2013; Perego et al., 2012). We follow this

August 30, 2024

427   practice except that here the discretization originates from a variational principle. This
428   has a number of advantages (see §2.3 and DPL, 2010). The following is a brief outline of
429   the finite element discretization. Additional details about the grid and the associated
430   discretization are provided in Appendix B. For simplicity, we confine ourselves to two
431   dimensions with coordinates (x,z) and velocities (u,w). Generalization to three
432   dimensions is possible (an example of a three-dimensional grid appropriate for our
433   purpose is discussed in Appendix B). Further, we discuss only the case of direct
434   substitution for basal boundary conditions in the variational functional, i.e., (15) or (33).
435   The remarks in this Section will apply to both the standard and transformed Stokes
436   models; for example, the discrete pressure variable p may refer to either the standard
437   pressure P or the transformed pressure $\tilde{P}$.
438

439   Consider an arbitrary grid with a total of $N = n_u + n_w + n_p$ unknown discrete
440   variables at appropriate nodal locations $1 \le i \le N$, with n_u horizontal velocity variables,
441   n_w vertical velocity variables, and n_p pressure variables, so that

442    $$V = \left\{ V_1, V_2, \cdots, V_N \right\}^T = \left\{ \left\{ u_1, u_2, \cdots, u_{n_u} \right\}, \left\{ w_1, w_2, \cdots, w_{n_w} \right\}, \left\{ p_1, p_2, \cdots, p_{n_w} \right\} \right\}^T = \left\{ u, w, p \right\}^T \quad (44)$$

443   is the vector of all the unknown discrete variables that are the degrees of freedom of the
444   model. If using Lagrange multipliers for basal boundary conditions then discrete
445   variables corresponding to λ_z, Λ must be added. Variables are expanded in terms of
446   shape functions $N_i^k(\mathbf{x})$ associated with each nodal variable i in each element k, so that
447    $V^k(\mathbf{x}) = \sum_i V_i N_i^k(\mathbf{x})$ is the spatial variation of all variables in element k, summed over
448   all variable nodes located in element k. Shape functions associated with a given node
449   may differ depending on the variable (i.e., $u, w,$ or p). Substituting into the functional,
450   (15) or (33), integrating and assembling the contributions of all elements, we obtain a
451   discretized variational functional in terms of the nodal variable vectors u, w, p, as follows

452    $$\mathcal{A}(u, w, p) = \sum_k \mathcal{A}^k(u, w, p), \quad (45)$$

453   where $\mathcal{A}^k(u, w, p)$ is the local functional evaluated by integrating over element k. Since
454   the term in the functional involving the product of pressure and divergence of velocity is

455 linear in pressure and velocity, and the term responsible for gravity forcing is linear in
456 velocity, the functional (45) may be written in matrix form as follows

$$\mathcal{A}(u,w,p) = \mathcal{M}(u,w) + p^T\left(M_{UP}^T u + M_{WP}^T w\right) + u^T F_U + w^T F_W , \qquad (46)$$

458 where the notation from (44) has been used, i.e., $u = \left\{u_1, u_2, \cdots, u_{n_u}\right\}^T$, etc. Parentheses

459 indicate a functional dependence on the indicated variables. Comparison with (15) and

460 (33) indicates that $\mathcal{M}(u,w)$ is a nonlinear positive-definite function of the velocity

461 components u, w, M_{UP}^T, M_{WP}^T are constant $n_p \times n_u$ and $n_p \times n_w$ matrices, respectively,

462 arising from the incompressibility constraint, and F_U, F_W are constant gravity forcing

463 vectors, of dimension n_u and n_w, respectively. Note that $F_U = 0, F_W \neq 0$ specifies the

464 standard Stokes model, and $F_U \neq 0, F_W = 0$ the transformed Stokes model. The discrete

465 functional $\mathcal{M}(u,w)$ differs but it remains positive-definite in both.

466

467   Discrete variation of the functional corresponds to partial differentiation with

468 respect to each of the discrete variables in V . Thus, the discrete Euler-Lagrange

469 equations that correspond to the u-momentum, w-momentum, and continuity equations,

470 respectively, are given by

$$471 \qquad R(u,w,p) = \begin{bmatrix} R_U(u,w,p) \\ R_W(u,w,p) \\ R_P(u,w) \end{bmatrix} = \begin{bmatrix} \mathcal{M}_U(u,w) + M_{UP}p + F_U \\ \mathcal{M}_W(u,w) + M_{WP}p + F_W \\ M_{UP}^T u + M_{WP}^T w \end{bmatrix} = 0 , \qquad (47)$$

472 where $R(u,w,p)$ is the residual vector with components $R_U(u,w,p) = \partial\mathcal{A}/\partial u$,

473 $R_W(u,w,p) = \partial\mathcal{A}/\partial w$, and $R_P(u,w) = \partial\mathcal{A}/\partial p$. The functionals $\mathcal{M}_U(u,w) = \partial\mathcal{M}/\partial u$,

474 $\mathcal{M}_W(u,w) = \partial\mathcal{M}/\partial w$ are nonlinear vectors of dimension n_u and n_w , respectively.

475 Altogether, (47) is a set of N equations for the N unknown discrete variables V_i. As

476 explained previously, all boundary conditions are already included in functional (46), and

477 therefore are also incorporated into the discrete Euler-Lagrange equations (47).

478

479   Since the overall system (47) is nonlinear, it is typically solved using Newton-

480 Raphson iteration, expressed in matrix notation as follows

August 30, 2024

481
$$M\left(u^K, w^K\right)\Delta V + R\left(u^K, w^K, p^K\right) = 0,\qquad(48)$$

482 where K is the iteration index, $M(u,v) = \partial^2 \mathcal{A}(V)/\partial V_i\,\partial V_j$ is a symmetric $N \times N$

483 Hessian matrix, and ΔV is the column vector given by

484
$$\Delta V = \left\{\Delta u, \Delta w, \Delta p\right\}^T = \left\{u^{K+1} - u^K, w^{K+1} - w^K, p^{K+1} - p^K\right\}^T.$$

485 Given V^K from the previous iteration, (48) is a linear matrix equation that is solved at

486 each iteration for the N new variables V^{K+1}. In view of (46) and (47), the Hessian

487 matrix $M(u,w)$ may be decomposed into several submatrices, as follows

488
$$M(u,w) = \begin{bmatrix} M_{UU}(u,w) & M_{UW}(u,w) & M_{UP} \\ M_{UW}^T(u,w) & M_{WW}(u,w) & M_{WP} \\ M_{UP}^T & M_{WP}^T & 0 \end{bmatrix}.\qquad(49)$$

489 Submatrices $M_{UW}(u,w) = \partial^2 \mathcal{M}/\partial u\,\partial w$, etc., depend nonlinearly on u, w. Thus,

490 $M_{UU}(u,w), M_{WW}(u,w)$ are square $n_u \times n_u$, $n_w \times n_w$ symmetric matrices, respectively,

491 while $M_{UW}(u,w)$ is a rectangular $n_u \times n_w$ matrix since n_u, n_w may not be equal. As noted

492 earlier, M_{WP}^T is an $n_p \times n_w$ matrix and therefore not square unless $n_p = n_w$.

493

494 **4.2 Blatter-Pattyn Discretizations**

495

496 For completeness, we express the Blatter-Pattyn approximations from §3.4 in matrix

497 form, as follows

498   (1) The standard Blatter-Pattyn model from §3.4.1 takes the simple form

499
$$R^{BP}(u) = \mathcal{M}_U(u,0) + F_U = 0,\qquad(50)$$

500 whose Newton-Raphson iteration is given by

501
$$M^{BP}\left(u^K\right)\Delta u + R^{BP}\left(u^K\right) = 0,\qquad(51)$$

502 and therefore the Blatter-Pattyn Hessian matrix is given by $M^{BP}(u) = M_{UU}(u,0)$.

August 30, 2024

503   (2) The extended Blatter-Pattyn approximation from §3.4.2 becomes

504
$$R^{EBP}(u,w,p) = \begin{bmatrix} \mathcal{M}_U(u,0) + M_{UP}p + F_U \\ M_{WP}p \\ M_{UP}^T u + M_{WP}^T w \end{bmatrix} = 0 \,, \tag{52}$$

505   with the Newton-Raphson iteration given by

506
$$M^{EBP}(u^K)\Delta V + R^{EBP}(u^K, w^K, p^K) = 0 \,, \tag{53}$$

507   and the associated Hessian matrix is

508
$$M^{EBP}(u) = \begin{bmatrix} M_{UU}(u,0) & 0 & M_{UP} \\ 0 & 0 & M_{WP} \\ M_{UP}^T & M_{WP}^T & 0 \end{bmatrix} . \tag{54}$$

509

510 **4.3 Solvability Issues**

511 **4.3.1 Solvability of Stokes and Blatter-Pattyn Models**

512

513 We now consider the solution of the three linear matrix problems (48), (51), (53)

514 associated with the Stokes and the corresponding Blatter-Pattyn approximate models.

515 While there are no issues in the continuous case, this is not so in the discrete case

516 depending on the choice of the grid and the finite elements, as noted earlier. The discrete

517 system to be solved has the general form

518
$$\mathbf{M}\left\{ \begin{array}{c} \mathbf{u} \\ p \end{array} \right\} = \begin{bmatrix} A & B \\ B^T & 0 \end{bmatrix} \left\{ \begin{array}{c} \mathbf{u} \\ p \end{array} \right\} = \left\{ \begin{array}{c} \mathbf{f} \\ g \end{array} \right\} \,, \tag{55}$$

519 where $\mathbf{u} = \{u,w\}^T$ in the linear case or $\{\Delta u, \Delta w\}^T$ in the nonlinear case, and similarly for

520 the vector of pressures or pressure increments p. The form (55) is characteristic of

521 Stokes-type problems, or more generally of constrained minimization problems using

522 Lagrange multipliers. In finite element terminology these are called "mixed" or "saddle

523 point" problems, meaning that velocity components and the pressure occupy different

524 finite element spaces, and that the solution of (55) is actually at the saddle point with

525 respect to the velocity and pressure variables of the quadratic form associated with (55).

526 The matrix $\mathbf{M}$ is symmetric but indefinite, with both positive and negative eigenvalues.

527 As a result, the matrix inverse may not be bounded and may lack stability.

528

529   There are three cases to consider:

530   (1) The standard Blatter-Pattyn model, (51). In this case only the matrix A

531   exists, it is elliptic, and $B = B^T = 0$. As a result, the standard Blatter-Pattyn model is a

532   well-behaved and stable unconstrained minimization problem. The model (51) is self-

533   contained and is solved for u while the vertical velocity w is potentially available a

534   posteriori from a separately obtained continuity equation.

535   (2) The extended Blatter-Pattyn model, (53), (54). The middle row of the Hessian

536   (54) indicates that the solution for the pressure will be zero. Using this in the top row of

537   the Hessian, one obtains the standard Blatter-Pattyn system and therefore the same well-

538   behaved horizontal velocity u as above, with the result that the bottom row of the

539   Hessian, the continuity equation, is the only way to obtain a solution for the vertical

540   velocity w. However, this is possible only if matrix M_{WP}^T is invertible, which at

541   minimum requires a square matrix, i.e., $n_p = n_w$, and this depends on the finite element

542   grid chosen for the discretization. For example, the popular second-order Taylor-Hood

543   (P2-P1) element with piecewise quadratic velocity and linear pressure (Hood and Taylor,

544   1973) typically has $n_p \ll n_w$. As a result, the linear system for w is greatly

545   underdetermined and cannot be solved for w. In fact, this is a problem for all inf-sup

546   stable elements with $n_p \neq n_w$, such as the Taylor-Hood element, for example.

547   (3) The standard and transformed Stokes models, (48), (49). These models

548   require the use of pressure as a Lagrange multiplier to enforce incompressibility and

549   therefore these are mixed or saddle point problems, as mentioned previously. To avoid

550   problems with the solution these finite elements must satisfy a certain condition, the

551   Ladyzhenskaya–Babuška–Brezzi (LBB, or inf-sup) condition. There is a very large

552   literature on the subject, e.g., Boffi et al. (2008), Elman et al. (2014), Auricchio et al.

553   (2017). Both the standard and transformed Stokes models are subject to this problem and

554   in general must use inf-sup stable finite elements. Testing for stability is not trivial.

555   However, collections of inf-sup stable elements for the Stokes equations may be found in

556   many papers and books on mixed methods, e.g., Boffi et al. (2008). The popular second-

557   order Taylor-Hood P2-P1 element (Hood and Taylor, 1973) is an example of an inf-sup

558   stable element. Some results involving this element are shown in Fig. 13 for Test B, one

559   of the test problems described in Appendix A.

560

4.3.2 A Special Case: Invertible Continuity Equation

In the continuous case, the Blatter-Pattyn approximation (§3.4.1) implies that vertical velocity w is obtainable from the continuity equation after having solved for the horizontal velocities u, v. As mentioned previously, this is possible to do in the continuum but not necessarily so in the discrete case. The 2D discrete continuity equation from (47) or (52) is given by

$$M_{UP}^T u + M_{WP}^T w = 0 . \tag{56}$$

For this to be solvable for w in terms of the horizontal velocity, i.e., $w(u)$, means that matrix M_{WP}^T must be invertible and thus it must be square and full rank. Since in general M_{WP}^T is an $n_p \times n_w$ matrix, for solvability at minimum this requires that

$$n_p = n_w . \tag{57}$$

Assuming that we are dealing with reasonable discretizations, we shall presume for our discussion that matrix M_{WP}^T is always full rank. If Lagrange multipliers were to be used, this means that the number of unknown pressures n_p would have to be augmented by the number of Lagrange multipliers so (57) would become $n_p + \lambda_z + \Lambda = n_w$ (See Appendix B, §B2, for more details). We shall refer to (57) (together with the assumption of full rank) as the solvability condition. In Appendix B we present several grids and elements that satisfy this condition, including one variant in particular, the P1-E0 element, that will be used in most of the 2D test problems featured in this paper. Thus, if the solvability condition is satisfied, the discrete continuity equation (56) may be inverted for the vertical velocity, to obtain

$$w(u) = -M_{WP}^{-T} M_{UP}^T u , \tag{58}$$

where matrix M_{WP}^{-T} is defined by

$$M_{WP}^{-T} = \left(M_{WP}^T \right)^{-1} = \left(M_{WP}^{-1} \right)^T . \tag{59}$$

Here wee have used the fact that if matrix M_{WP}^T is invertible then so is its transpose M_{WP}. Note that (58) is one discrete form of equation (43).

      Invertibility of the continuity equation has several important applications. First, it is a necessary requirement for the new Stokes approximations that are discussed in §6.2.

591   Since these approximations are based on approximating the vertical velocity in the

592   transformed second invariant, (28), it is necessary to obtain the vertical velocity

593   independently of solving the entire coupled Stokes problem. Second, we noticed earlier

594   that the extended Blatter-Pattyn model does not work with a Taylor-Hood P2-P1 grid

595   because the solvability condition is not satisfied. However, this model does work with a

596   variant of the Taylor-Hood grid, the P2-E1 grid, illustrated in Fig. 13A, which does

597   satisfy the solvability condition and this therefore allows for a successful calculation of

598   the vertical velocity.

599

600   Perhaps the main reason for the importance of the solvability condition is that it

601   implies that the Stokes variational principle, (15) or (33), may be transformed into and

602   therefore that it is equivalent to an optimization or minimization problem. Consider the

603   discrete form of the variational functional given by (46). Working with a grid that

604   satisfies the solvability condition, we may substitute the vertical velocity given by (58)

605   into the functional (46). This immediately eliminates the term responsible for the

606   continuity equation, including the pressure, and one obtains a functional in terms of

607   horizontal velocity u only, as follows

608   $$\mathcal{A}(u) = \mathcal{M}(u, w(u)) + u^T F_U + w(u)^T F_W.\tag{60}$$

609   Since the functional $\mathcal{M}(u, w(u))$ is positive semi-definite, this is now an unconstrained

610   minimization problem, entirely analogous to the standard Blatter-Pattyn problem of

611   §3.4.1 except that here it represents the full Stokes problem for either the standard (F_W)

612   or the transformed (F_U) formulation. This result suggests that a conventional Stokes

613   problem, when solved on a grid satisfying the solvability condition, is equivalent to an

614   unconstrained minimization problem and therefore is well behaved. This is because any

615   problem will give the same answer whether formulated as (46) or (60) on a grid that

616   satisfies the solvability condition.

617

618   Note that functional (60) is actually the discrete version of a pressure-free

619   formulation that was attempted analytically by Dukowicz (2012). It is possible to

620   consider solving problems in practice using the pressure-free formulation (60) instead of

621   a standard saddle point formulation such as (46) or (47). However, this produces a dense

622   Hessian matrix that makes a solution using Newton-Raphson iteration very costly and

623   therefore impractical, particularly for large problems.

624

August 30, 2024

5. Comparison of the Standard and Transformed Stokes Models

The standard and transformed Stokes models are expected to converge to the same solution. To verify that this is indeed the case we do a number of calculations for some 2D test problems based on the ISMIP-HOM benchmark (Pattyn et al, 2008). These tests are described in Appendix A where they are referred to as Test B and Test D*. Test B involves no-slip boundary conditions on a sinusoidal bed, and Test D* evaluates sliding of the ice sheet along a flat bed in the presence of sinusoidal friction. The tests are discretized using P1-E0 elements on a regular grid composed of n quadrilaterals in the x-direction and m quadrilaterals in the z-direction, illustrated in Fig. B1, with each quadrilateral divided into two triangles. Results are presented for two domain lengths, $L = 5$ km and 10 km, to test the aspect ratio range where the Blatter-Pattyn model begins to fail, and using a relatively coarse grid, i.e., $m = n = 40$, except when we consider the convergence of the models with grid refinement in Fig. 3.

Fig. 3 evaluates the convergence of the two Stokes models as a function of grid resolution r, where r is the number of quadrilaterals in either direction. The models do converge to the same solution and convergence is second order as expected from the use of linear elements. Interestingly, the transformed Stokes model displays considerably smaller error at all resolutions in Test B. As a result, we observe that standard Stokes calculations are not fully converged even at the 40x40 resolution.
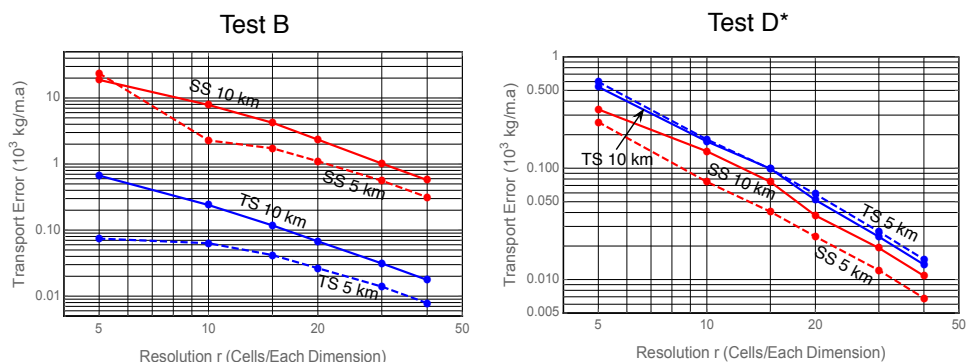
Figure 3. Convergence of ice transport in Tests B and D* with grid refinement. Transformed Stokes (TS) plots are in blue and standard Stokes plots (SS) are in red.

Fig. 4 shows the vertical profiles of the horizontal velocity u at outflow, $x = L$. We plot results from the no-slip Test B problem and the two frictional sliding problems, Tests D and D*. The Test D profile from the ISMIP-HOM benchmark is almost

August 30, 2024

653 vertically constant, indicating that the value for basal friction originally chosen is too
654 small. This is what motivated the change from Test D to Test D* in Appendix A.
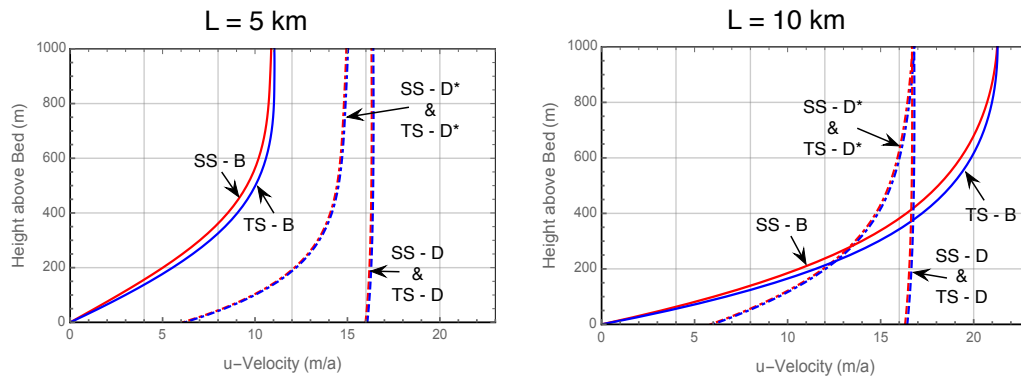
655

656 **Figure 4.** The u-velocity profile at location $x = L$ as a function of height from the bed.

657

658   Figs. 5 and 6 show the u-velocity at the ice sheet upper surface for Tests B and
659 D*. This is the benchmark used in ISMIP-HOM to compare the different ice sheet
660 models. Here we compare four cases: the standard Stokes model (SS), the transformed
661 Stokes model (TS), the Blatter-Pattyn (BP) model, and for reference, a very high
662 resolution full-Stokes Test B calculation "oga1" (SS-HR), available from the ISMIP-
663 HOM paper and also independently available in Gagliardini and Zwinger (2008). The TS
664 and the SS-HR plots lie on top of one another (they have been offset slightly for clarity),
665 indicating that the TS model is already fully converged. We again observe that the SS
666 model is not yet converged in Test B, particularly at $L = 5$ km. As also seen in the
667 ISMIP-HOM paper, the Blatter-Pattyn calculation (BP) shows large deviations from the
668 Stokes results, especially so at $L = 5$ km where the surface velocity is entirely out of
669 phase with the Stokes results. Test D* results in Fig. 6 for the SS and TS models are very
670 similar (the SS plot has been slightly offset upward for visibility). As expected, the error
671 in the Blatter-Pattyn results is noticeable at $L = 10$ km and very large at $L = 5$ km.

672

673   Pressure results are not shown because, particularly in the transformed case,
674 pressure has little or no physical significance. However, pressures calculated on the P1-
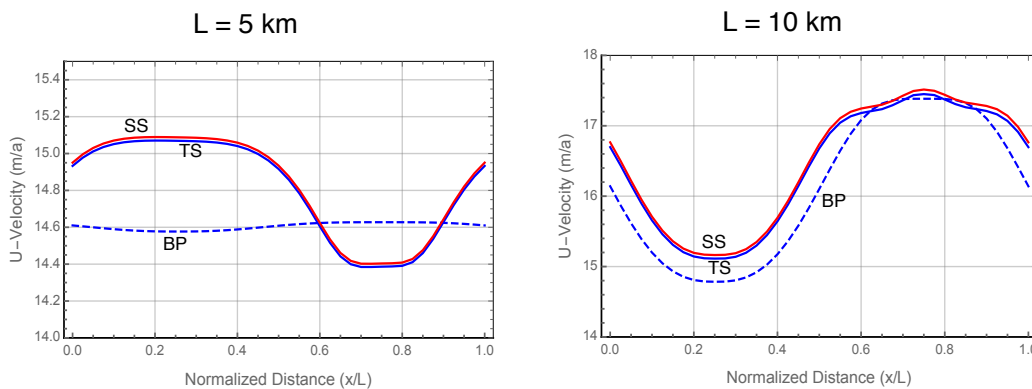675 E0 grid are particularly smooth and well behaved.

L = 5 km   **L = 10 km**
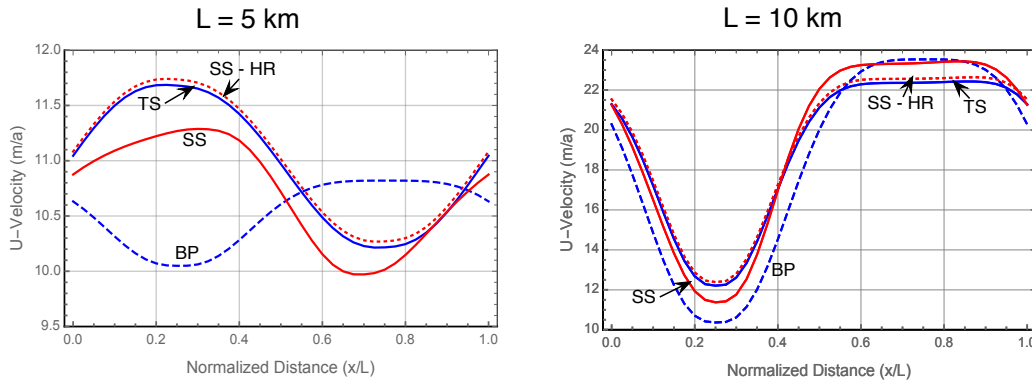
Figure 5. Upper surface u-velocity, $u(x, z_s)$ - Test B, No-slip boundary conditions.

L = 5 km   **L = 10 km**

Figure 6. Upper surface u-velocity, $u(x, z_s)$ - Test D*, Modified frictional sliding case.

6. Applications of the Transformed Stokes Model
6.1 Adaptive Switching between Stokes and Blatter-Pattyn Models

One way of reducing the cost of a full Stokes calculation is to use it adaptively with a cheaper approximate model. That is, one may use the cheaper model in those parts of a problem where it is accurate, and the more expensive full Stokes model where the approximate model loses accuracy. One example of such an adaptive approach is the tiling method by Seroussi et al. (2012). However, there are drawbacks to such methods, such as the difficulty of incorporating two or more presumably quite different models into a single model, and the additional complexity of a necessary transition zone to couple the disparate models.

The transformed Stokes model used in such an adaptive role is attractive because it may be switched between the Stokes and Blatter-Pattyn cases simply by switching the

August 30, 2024

696   parameter $\xi \in \{0,1\}$ between its two values. For simplicity the extended Blatter-Pattyn

697   approximation ($\xi = 0, \hat{\xi} = 1$) is being used since both the Stokes and the Blatter-Pattyn

698   parts of the code have the same number of discrete variables. The extended Blatter-

699   Pattyn model requires the use of a grid that satisfies the solvability condition as explained

700   in §4.3. We therefore use the P1-E0 element. However, it would be computationally

701   cheaper to use the standard Blatter-Pattyn approximation ($\xi, \hat{\xi} = 0$) instead, solving only

702   for the horizontal variables and coupling to the Stokes model with $p = 0$ and $w = w(u, v)$

703   at the interface. This, however, implies much more complicated programming.

704

705   To demonstrate the idea of adaptive switching with a transformed Stokes model,

706   we introduce a new test problem, Test O, described in Appendix A and illustrated in Fig.

707   A1. This consists of an inclined ice slab whose movement is obstructed by a thin

708   obstacle protruding 20% of the ice depth up from the bed. No-slip boundary conditions

709   are applied along the bed and on the obstacle itself. Because of the localized nature of

710   the obstacle, the Blatter-Pattyn approximation conditions, (38), must fail near the obstacle

711   and therefore the full Stokes model is needed for good accuracy, at least locally.
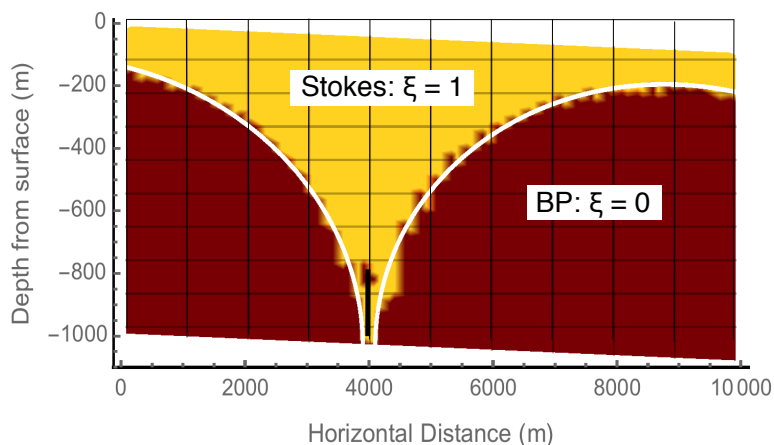
712

713   **Figure 7.** Mask function (white curve, $z = F_M(x)$) to indicate where the Stokes and BP

714   models are activated in the 20% obstacle test problem. The dark brown region delineates

715   the region where $|\partial w / \partial x| \leq 0.1 |\partial u / \partial z|$ in a Blatter-Pattyn calculation.

716

717   To implement this, we first use a Blatter-Pattyn calculation to outline regions

718   where $|\partial w / \partial x| \leq 0.1 |\partial u / \partial z|$, approximately localizing where the Blatter-Pattyn

August 30, 2024

719   approximation is valid. This determines a mask function $z = F_M(x)$, illustrated in Fig. 7

720   by the white curves, that specifies where the two models must be used. Defining the

721   centroid of a triangular element by (x_C, z_C), the code makes a selection in each element:

722
$$z_C \leq F_M(x_C) \quad \Rightarrow \quad \text{Set } \xi = 0, \quad \text{i.e., the Blatter-Pattyn region,}$$
$$z_C > F_M(x_C) \quad \Rightarrow \quad \text{Set } \xi = 1, \quad \text{i.e., the Stokes region.}$$

723   Somewhat counterintuitively, the Stokes region occupies the upper part of the domain in

724   Fig. 7 and includes the obstacle, while the Blatter-Pattyn region occupies much of the

725   bottom part of the domain. A transition zone, e.g., $0 \leq \xi(x,z) \leq 1$, is possible but was not

726   used in the present calculation.
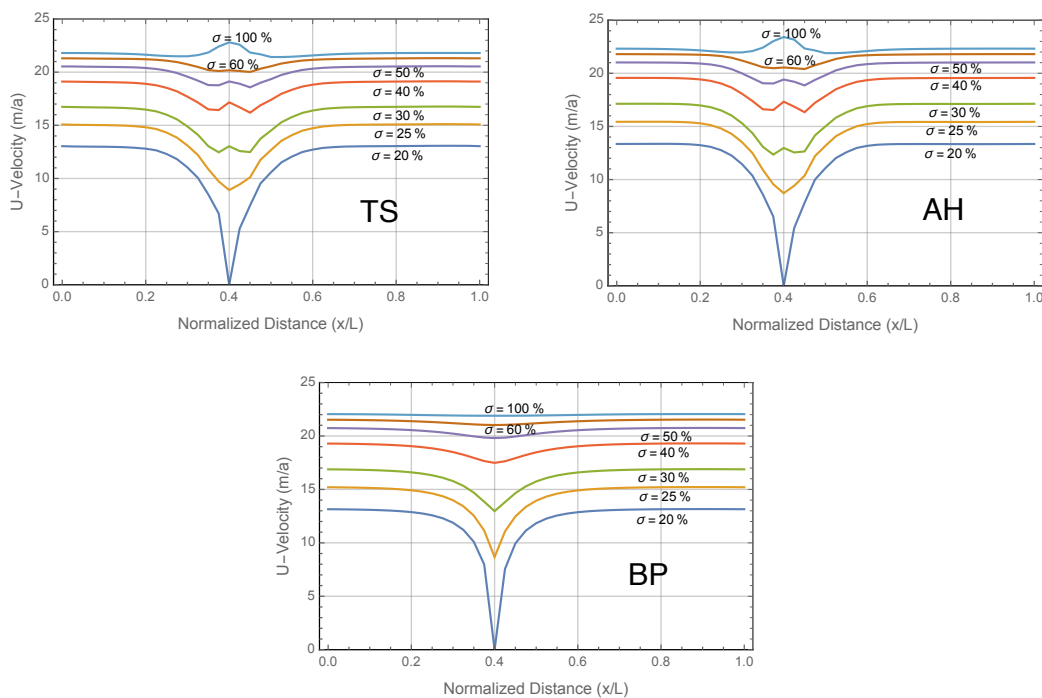
727
728   **Figure 8.** Comparing results for the Transformed Stokes (TS),

729   the Adaptive-Hybrid (AH), and the Blatter-Pattyn (BP) models in Test O.

730

731   The Adaptive-Hybrid results are shown in Fig. 8, which shows curves of the

732   horizontal velocity u at seven different vertical positions specified as a percentage of the

733   distance between top and bottom, with $\sigma = 100\%$ at the top surface. The top right panel

734   shows the results for the adaptive-hybrid model (AH). For comparison, the top left panel

735   and the bottom panel show results for the Stokes (TS) and the Blatter-Pattyn (BP)

736   calculations, respectively. All calculations are at the 40x40 resolution. The Adaptive-

737   Hybrid results are very similar to the full Stokes results, reproducing most features of the

738 velocity profiles, including the velocity bump at the top surface, indicating that even the
739 top surface feels the presence of the obstacle. The Blatter-Pattyn results are much less
740 accurate; they completely miss the details of the flow near the obstacle. We also measure
741 the RMS error in the u-velocity relative to the Stokes results. The RMS error in the
742 Blatter-Pattyn case is 0.493 m/a and 0.440 m/a in the Adaptive-Hybrid case, smaller in
743 the Blatter-Pattyn case as expected, but the difference is not as large and striking as the
744 visual difference in Fig. 8. Nevertheless, the adaptive-hybrid method is successful
745 judged by the Fig. 8 results alone. Unfortunately, an estimate of the computational cost
746 savings will have to wait a more realistic implementation.

747

748 **6.2. Two Stokes Approximations Beyond Blatter-Pattyn**

749

750 As shown in §3.4, simply setting $w = 0$ in the second invariant $\tilde{\varepsilon}^2$ in the transformed

751 functional $\tilde{\mathcal{A}}$ results in the standard Blatter-Pattyn approximation. This suggests that

752 approximating the vertical velocity w in the functional would be a good way to create

753 approximations that improve on the Blatter-Pattyn approximation since $w = 0$ already

754 produces an excellent approximation. We will look at two such methods in this Section

755 although others are possible. The first method, to be called the BP+ approximation, is

756 implemented using a combination of Newton and Picard iterations such that at each

757 Newton iteration the pressure-free variational functional is evaluated using a lagged

758 vertical velocity w^K from the previous iteration. The pressure is used in a subordinate

759 role as a "test function" to obtain a decoupled invertible continuity equation to obtain

760 $w(u^K)$. Although this method improves on the accuracy of the Blatter-Pattyn

761 approximation, its overall accuracy is limited because it uses only the horizontal

762 momentum equation and neglects the vertical momentum equation. The second method,

763 to be called the Dual-Grid approximation, keeps the pressure and vertical velocity as in

764 the transformed Stokes model but approximates it by discretizing the continuity equation

765 on a coarser grid. Since vertical velocity w is determined by inverting the continuity

766 equation, this has the effect of approximating the vertical velocity while reducing the

767 number of pressure and vertical velocity variables. This preserves the structure of the

768 Stokes model, while the degree of approximation is determined by the amount of

769 coarsening of the continuity grid.

770

August 30, 2024

771   **6.2.1 An Improved Blatter-Pattyn or BP+ Approximation**

772

773   To prepare, we introduce a pair of 2D variational quasi-functionals, $\tilde{\mathcal{A}}_{PS1}[u]$ and

774     $\tilde{\mathcal{A}}_{PS2}[\tilde{P}]$. Noting that $\tilde{P} = 0$ in the Blatter-Pattyn approximation, we drop the pressure

775   term from the transformed functional (33) and define a new pressure-free functional,

776
$$\tilde{\mathcal{A}}_{PS1}[u] = \int_V dV \left[\frac{4n}{n+1} \eta_0 \left(\tilde{\varepsilon}^2 \right)^{(1+n)/2n} + \rho g u \frac{\partial z_s}{\partial x} \right] \\ + \frac{1}{2} \int_{S_{B2}} dS \, \beta(x) \left(u^2 + \zeta \left(u n_x / n_z \right)^2 \right), \tag{61}$$

777   where

778
$$\tilde{\varepsilon}^2 = \left(\frac{\partial u}{\partial x} \right)^2 + \frac{1}{4} \left(\frac{\partial u}{\partial z} + \frac{\partial w}{\partial x} \right)^2. \tag{62}$$

779   Since the continuity equation has been eliminated from (61), incompressibility is

780   introduced separately by defining a second functional,

781
$$\tilde{\mathcal{A}}_{PS2}[p] = \int_V dV \, p \left(\frac{\partial u}{\partial x} + \frac{\partial w}{\partial z} \right). \tag{63}$$

782   Note that functional (61) is a function of u, w but variation is to be taken only with

783   respect to u, and similarly, functional (63) is a function of u, w, p but variation is taken

784   only with respect to p. Direct substitution is used for boundary conditions, as before.

785   Here we are effectively viewing the pressure p as a "test function" in the finite element

786   sense. This gives us great flexibility to create elements that satisfy the solvability

787   condition (57) as desired. In a triangulation, for example, pressures may be assigned to

788   every two triangles, as in a P1-E0 grid, while others may be assigned to a single triangle

789   so as to achieve an equal number of pressure and vertical velocity variables.

790

791   The variation of $\tilde{\mathcal{A}}_{PS1}[u]$ with respect to u, results in a set of n_u discrete Euler-

792   Lagrange equations,

793
$$\hat{R}_U(u,w) = \frac{\partial \tilde{\mathcal{A}}_{PS1}(u,w)}{\partial u} = M_U(u,w) + F_U = 0. \tag{64}$$

794   This may be recognized as the Blatter-Pattyn model, (50), when w is set to zero. The

795   discrete variation of $\tilde{\mathcal{A}}_{PS2}[p]$ with respect to p, results in the continuity equation, (56),

796
$$\hat{R}_P(u,w) = \frac{\partial \tilde{\mathscr{A}}_{PS2}(u,w,p)}{\partial p} = M_{UP}^T u + M_{WP}^T w = 0 \ . \tag{65}$$

797 These two systems are now combined to form the BP+ approximation, as follows

798
$$\hat{R}(u,w) = \left[\hat{R}_U(u,w), \hat{R}_P(u,w) \right]^T = 0 \ . \tag{66}$$

799 This is a single system of $n_u + n_p$ equations to determine the $n_u + n_w$ discrete variables

800 u, w, implying that (66) is viable only on grids satisfying the solvability condition,

801 $n_p = n_w$. Just as in the standard Blatter-Pattyn approximation in §3.4.1, the vertical

802 momentum equation is missing, but instead of neglecting w, the vertical velocity is now

803 consistently obtained from the continuity equation.

804

805 The continuum version of the discrete Euler-Lagrange system (64), (65) may be

806 written as follows

807
$$\frac{\partial}{\partial x}\left(4\tilde{\mu}\frac{\partial u}{\partial x} \right) + \frac{\partial}{\partial z}\left(\tilde{\mu}\left(\frac{\partial u}{\partial z} + \frac{\partial w}{\partial x} \right) \right) - \rho g \frac{\partial z_s}{\partial x} = 0,$$
$$\frac{\partial u}{\partial x} + \frac{\partial w}{\partial z} = 0, \tag{67}$$

808 whose the boundary conditions are

809
$$4\tilde{\mu}\frac{\partial u}{\partial x}n_x + \tilde{\mu}\left(\frac{\partial u}{\partial z} + \frac{\partial w}{\partial x} \right)n_z = 0 \ \text{on} \ S_S, \quad u = w = 0 \ \text{on} \ S_{B1},$$
$$\left. \begin{array}{l} 4\tilde{\mu}\frac{\partial u}{\partial x}n_x + \tilde{\mu}\left(\frac{\partial u}{\partial z} + \frac{\partial w}{\partial x} \right)n_z + \beta(x)\left(u + \zeta u\left(n_x/n_z \right)^2 \right) = 0, \\ w = -u\,n_x/n_z, \end{array} \right\} \ \text{on} \ S_{B2}, \tag{68}$$

810 where $\tilde{\mu} = \eta_0\left(\tilde{\varepsilon}^2 \right)^{(1-n)/2n}$ and the second invariant $\tilde{\varepsilon}^2$ is given by (62). Remarkably, a

811 model exactly equivalent to (67), i.e., the BP+ approximation, was introduced by

812 Herterich (1987) to study the transition zone between an ice sheet and an ice shelf[1]. This

813 predates the less accurate, widely used Blatter-Pattyn model by some eight years.

814 Unfortunately, this anticipatory work seems to have faded into obscurity.

815

816 There are two ways of solving the BP+ system (66), as follows

---

[1] Reference pointed out to me by C. Schoof.

August 30, 2024

817   (1) <u>BP+, Quasi-variational, Newton iteration version</u>:

818   Although a single variational principle does not exist in this case, it is still

819   possible to make use of Newton-Raphson iteration to obtain second order convergence.

820   To do this, we treat (66) as a single multidimensional nonlinear system and solve it using

821   Newton-Raphson iteration, as follows

822
$$
\begin{bmatrix} M_{UU}\left(u^K, w^K\right) & M_{UW}\left(u^K, w^K\right) \\ M_{UP}^T & M_{WP}^T \end{bmatrix} \begin{bmatrix} \Delta u \\ \Delta w \end{bmatrix} + \begin{bmatrix} \hat{R}_U\left(u^K, w^K\right) \\ \hat{R}_P\left(u^K, w^K\right) \end{bmatrix} = 0 , \qquad (69)
$$

823   where $M_{UU}\left(u,w\right) = \partial \hat{R}_U\left(u,w\right)/\partial u$ and $M_{UW}\left(u,w\right) = \partial \hat{R}_U\left(u,w\right)/\partial w$ are the same

824   matrices as appear in (49). Convergence is rapid (quadratic) once in the basin of

825   attraction but each step is more expensive than the Picard iteration described next.

826

827   (2) <u>BP+, Newton/Picard iteration version</u>:

828   A single step of the Newton-Raphson system (69) may be written as follows

829
$$
\begin{aligned}
M_{UU}\left(u^K, w^K\right)\Delta u + M_{UW}\left(u^K, w^K\right)\Delta w + \hat{R}_U\left(u^K, w^K\right) &= 0, \\
M_{UP}^T u^{K+1} + M_{WP}^T w^{K+1} &= 0.
\end{aligned} \qquad (70)
$$

830   If we lag the vertical velocity, i.e., $w^{K+1} = w^K \Rightarrow \Delta w = 0$ in the first equation, we obtain a

831   Picard iteration algorithm as follows

           Starting from $K = 0$, choose an initial guess, $u^0 \neq 0, w\left(u^0\right),$

             Solve:

832
$$
\begin{aligned}
M_{UU}\left(u^K, w^K\right)\Delta u + \hat{R}_U\left(u^K, w^K\right) &= 0, \\
u^{K+1} &= u^K + \Delta u, \\
w^{K+1} = w\left(u^{K+1}\right) &= -M_{WP}^{-T} M_{UP}^T u^{K+1}, \\
K &= K+1,
\end{aligned} \qquad (71)
$$

           Repeat until convergence.

833   Each step of this iteration is inexpensive since it is equivalent to a step of the standard

834   Blatter-Pattyn model, (36). On the other hand, Picard iterations typically converge only

835   linearly. It remains to be seen which version is preferable in practice.

836

837   Both BP+ versions converge to the same solution. Fig. 9 compares the upper

838   surface u-velocity from the improved Blatter-Pattyn (BP+) approximation to the standard

839   Blatter-Pattyn approximation and to a reference exact Stokes calculation. The RMS u-

840   Error of the BP+ approximation relative to the exact Stokes case is shown in Fig. 12. The

August 30, 2024

841   BP+ approximation is noticeably more accurate than the BP approximation, particularly

842   in the $L = 5$ km case where the Blatter-Pattyn solution bears no resemblance to the

843   correct solution while the BP+ approximation shows excellent accuracy. This is

844   confirmed by the RMS u-Error results in Fig. 12 where BP+ is two to three times as

845   accurate as BP.
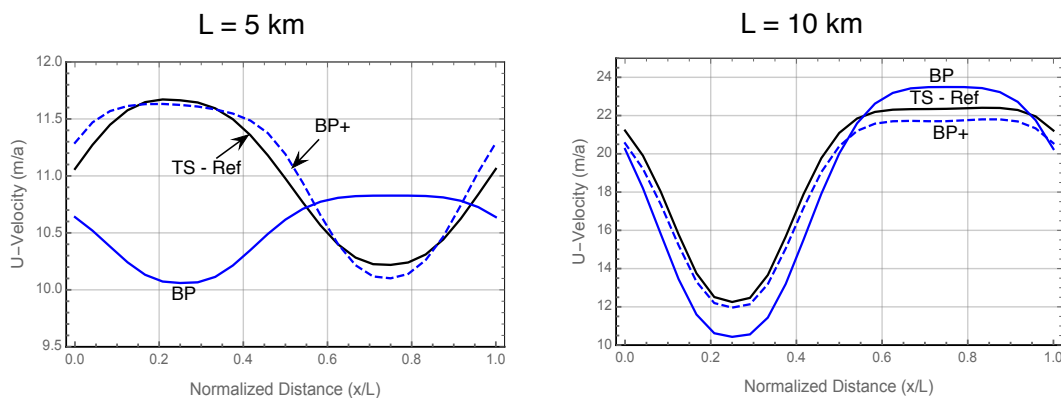
846

847   **Figure 9.** Comparing Approximations. Test B, Upper surface u-velocity.

848   TS-Ref: Transformed Stokes; BP: Blatter-Pattyn; BP+: Improved Blatter-Pattyn.

849   Resolution: 24x24.

850

851   These two versions depend on an invertible continuity equation to obtain

852    $w = w(u)$. However, vertical velocity w may already be available for the purpose of

853   temperature advection in production code packages that either incorporate or are based on

854   the Blatter-Pattyn approximation. Thus, the BP+ approximation, and particularly the

855   Newton/Picard version, may be attractive for use in such codes since they improve the

856   accuracy of the basic Blatter-Pattyn model, as seen in Fig. 9, at little additional cost.

857

858   **6.2.2 A "Dual-Grid" Transformed Stokes Approximation**

859

860   Here we take a different approach and approximate the continuity equation in the

861   transformed Stokes model, which indirectly approximates w. Thus, the continuity

862   equation is discretized on a grid coarser than the one used for the momentum equations,

863   and then interpolate the vertical velocity to appropriate locations on the finer grid. This

864   reduces the number of unknown variables in the problem, making it cheaper to solve but

865   hopefully without much loss of accuracy. As described in Appendix A, our test problem

866   grids are logically rectangular, divided into n cells horizontally and m cells vertically.

867   The coarse grid is constructed by dividing the fine grid into s equal segments in each

868   direction. This assumes that the integers n and m are each divisible by s, such that

869   there are nm/s^2 coarse cells in total, with each coarse cell containing s^2 fine cells. The

870   primary grid (i.e., the fine grid) was chosen to have $n = m = 24$, resulting in a reference

871   24×24 fine grid, so as to maximize the number of different coarse grids that may be

872   used for this test. Coarse grids were constructed using $s = 2, 3, 4, 6$, and this resulted in

873   fine/coarse grid combinations labeled by $24 \times 12, 24 \times 8, 24 \times 6, 24 \times 4$, respectively.

874   Similar to a P1-E0 fine grid, coarse grid vertical velocities w are located at vertices and

875   pressures at vertical edges. Fig. 10 illustrates the case of a single coarse and four fine

876   quadrilateral cells for a grid fragment with $n = m = 2$ and $s = 1$. For the Test B problem,

877   using direct substitution for basal boundary conditions, there will be nm u-variables and

878   nm/s^2 w- and p-variables each, for a total of $nm(1 + 2/s^2)$ unknown variables,

879   considerably fewer than the $3nm$ variables in the full resolution (i.e., fine grid) case,

880   depending on the value of s. The coarse grid terms in the functional that are affected,

881    $\tilde{P}(\partial u/\partial x + \partial w/\partial z)$ and $\partial w/\partial x$, are computed using coarse grid variables and

882   interpolated to the fine grid. We will consider two versions depending on how the coarse

883   grid terms are calculated and distributed on the fine grid.
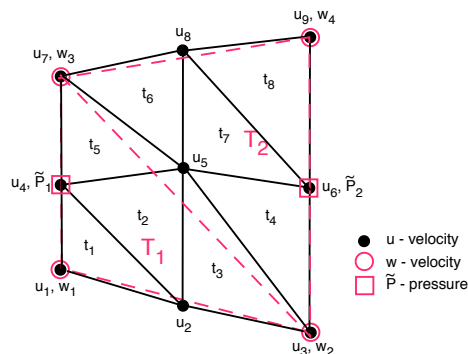
886   **Figure 10.** A Sample of a Coarse/Fine P1-E0 Grid for the Dual-Grid Approximation.

887   Resolution: $n = m = 2, s = 1$. Coarse grid is in red, fine grid in black.

889   (1) Approximation A, Bilinear interpolation:

890   Referring to Fig. 10, the four velocities at the vertices of the coarse grid

891   quadrilateral, i.e., u_1, u_3, u_7, u_9 and w_1, w_2, w_3, w_4, are used to obtain u, w at the remaining

892   five vertices of the fine grid by means of bilinear interpolation. Thus, the five velocities

893   u_2, u_4, u_5, u_6, u_8 are obtained in terms of vertex velocities u_1, u_3, u_7, u_9, and similarly for the

894   w velocities. The resulting complete set of fine grid variables, interpolated from coarse

August 30, 2024

895   grid variables, are used calculate the divergence $D = \left(\partial u/\partial x + \partial w/\partial z\right)$ and the quantity

896   $\partial w/\partial x$ in each of the eight triangular elements $t_1, t_2, \cdots, t_8$ of the fine grid. Coarse grid

897   pressures $\tilde{P}_1, \tilde{P}_2$ are associated with the coarse grid triangles T_1, T_2. The products $\tilde{P}_1 D$ in

898   elements t_1, t_2, t_3, t_5 and $\tilde{P}_2 D$ in elements t_4, t_6, t_7, t_8 are then accumulated over the entire

899   grid to obtain $\tilde{P}\left(\partial u/\partial x + \partial w/\partial z\right)$ for use in the transformed functional $\tilde{\mathcal{A}}$. Similarly, the

900   quantity $\partial w/\partial x$ is computed in the fine grid elements from coarse grid variables for use

901   in the second invariant $\tilde{\dot{\varepsilon}}^2$.

902

903   (2) <u>Approximation B, Linear interpolation</u>:

904   In this version, the three velocities at the vertices of the two coarse grid triangles

905   T_1 and T_2, i.e., u_1, u_3, u_7 and w_1, w_2, w_3 in T_1, and u_7, u_3, u_9 and w_3, w_2, w_4 in T_2,

906   approximate the divergence $D = \left(\partial u/\partial x + \partial w/\partial z\right)$ and the quantity $\partial w/\partial x$ as constant

907   values in the two coarse triangles. The constant quantities $\tilde{P}_1 D$, $\tilde{P}_2 D$ are then

908   accumulated over the entire grid. The constant quantity $\partial w/\partial x$ in each coarse triangle is

909   then distributed to each of the eight fine grid elements $t_1, t_2, \cdots, t_8$ depending on whether

910   the centroid of the fine triangular element is in T_1 or T_2. As in the previous case, this is

911   then used in the second invariant $\tilde{\dot{\varepsilon}}^2$ when evaluating the transformed functional $\tilde{\mathcal{A}}$.

912

913   While the number and type of unknown variables is the same in the two versions,

914   they differ considerably in accuracy, as is seen in Figs. 11 and 12. Fig. 11 compares the

915   upper surface u-velocity in both version, Approximations A and B, for the four coarse

916   grid combinations and the reference 24x24 fine grid calculation. Fig. 12 compares the

917   overall accuracy the same way by means of the RMS u-Error. As might be expected, the

918   accuracy of Approx. A is better than the accuracy of Approx. B, particularly in the case

919   when $L = 10$ km. Both versions are more accurate than the Blatter-Pattyn and BP+

920   approximations, except at the lowest 24x4 resolution when only the Approx. A version

921   retains that distinction.

August 30, 2024
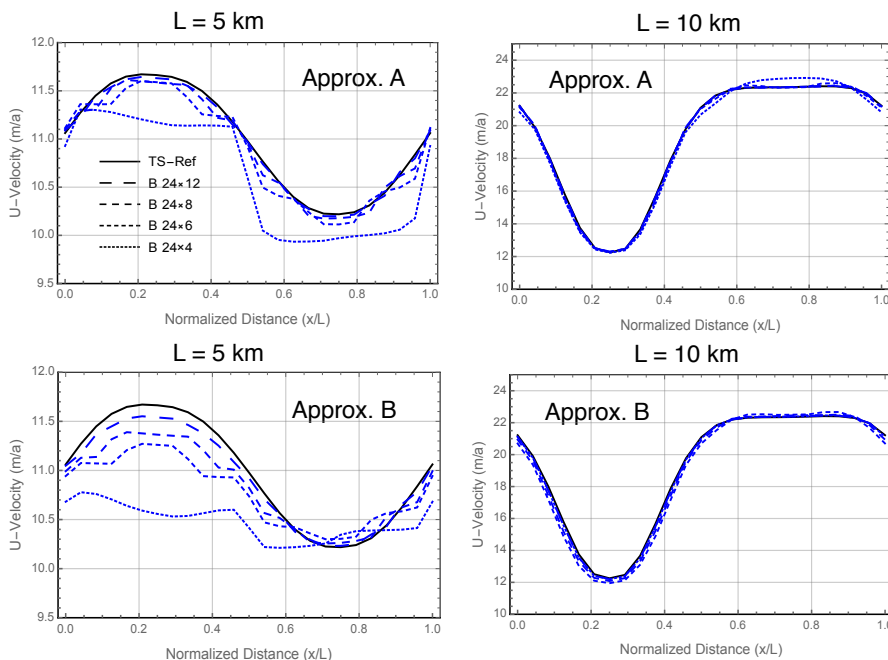
Figure 11. Comparing Approximations A and B. Test B. Upper surface u-velocity. TS-Ref: Reference Stokes 24x24; Fine/Coarse resolutions (r x R): 24xR, R=12, 8, 6, 4.

In summary, the dual-grid approximation improves on the Blatter-Pattyn approximation in both versions and at all resolutions, as seen in Fig. 12. Compared to the BP+ approximations, here the vertical momentum equation is retained, although in approximated form. In fact, here the solution procedure is very similar to that of the unapproximated Stokes model except that the dimensions of the pressure and the vertical velocity variables are reduced.
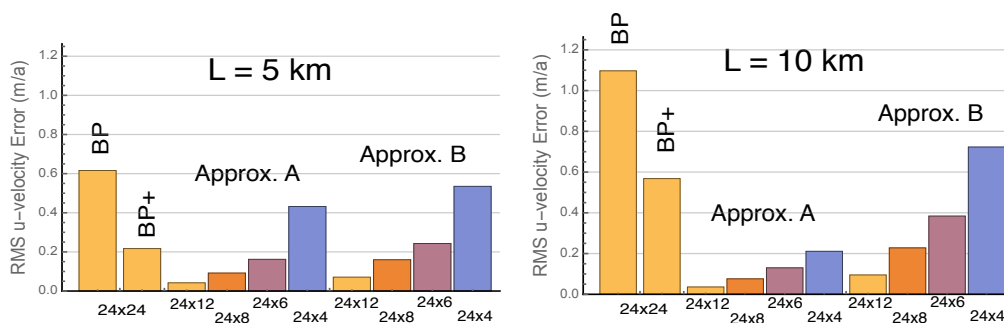
Figure 12. Comparing RMS u-Error in Different Approximations, Test B, Resolutions (r x R): Approx. BP, BP+: 24x24; Approx. A, B: 24xR, R=12, 8, 6, 4.

August 30, 2024

7. Second-Order Discretizations

So far we have been using first-order elements, primarily P1-E0. However, in current practice Stokes models are more often based on second-order elements such as the popular Taylor-Hood P2-P1 element (Leng et al., 2012; Gagliardini et al., 2013). In 2D the P2-P1 element, illustrated in Fig. 13A, has velocities on element vertices and edge midpoints and pressures on element vertices, resulting in a quadratic velocity and linear pressure distributions. The element satisfies the conventional inf-sup stability condition (e.g., Elman et al., 2014) but not the solvability condition (57). For example, in Test B with direct substitution for basal boundary conditions, the number of vertical velocity variables is $n_w = 4nm$, much larger than the number of pressure variables, $n_p = n(m+1)$.

Stokes models work well with a Taylor-Hood grid, as illustrated in Fig. 13, where both P2-P1 and P1-E0 models converge to a common Test B solution, but models that require the solvability condition (57) will not work on a P2-P1 grid, as is the case with the extended Blatter-Pattyn approximation. However, a second-order element can be constructed that is consistent with an invertible continuity equation. This is called the P2-E1 element and it is illustrated in Fig. 13A. It is second-order for velocities and linear for pressure, just like the P2-P1 element, but the pressure is edge-based, as in the P1-E0 element. Pressure is located midway between the velocities on the vertical cell edges, including an "imaginary" vertical edge joining the velocities in the middle of the vertical column. Since pressures are collinear with vertical velocities along vertical grid edges, as in the P1-E0 element, the same analysis in Appendix B demonstrates that this element also satisfies the solvability condition (57). As explained in Appendix B, this grid should be constructed using vertical columns of quadrilaterals. A 3D analog exists as explained in Appendix B.

Fig. 13B shows the approximate error of the ice transport as a function of grid refinement for the second-order P2-P1 and P2-E1 grids in transformed Stokes Test B calculations, together with similar results for the first-order P1-E0 grid from Fig. 3, for comparison. We note that both second order models show approximately the same error at resolution $r = 16$ as the first order P1-E0 model at resolution $r = 40$, and similarly for coarser resolutions such as $r = 8$ and $r = 20$, respectively. However, it is safe to say that these second-order calculations are considerably more expensive than the first-order calculations at comparable resolution or accuracy.

August 30, 2024
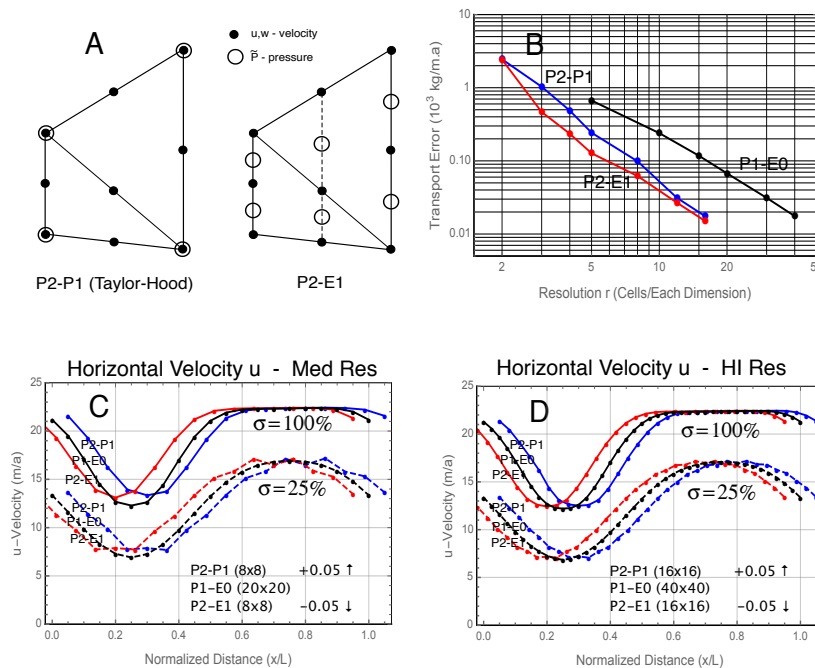
Figure 13. Comparing second-order discretizations based on the P2-P1 and P2-E1 elements from panel A to first-order discretizations using the P1-E0 element running Test B with L=10 km. Only transformed Stokes calculations are compared; standard Stokes results behave similarly. Panel B compares the convergence and accuracy of the various schemes with increasing resolution, while panels C, D compare the horizontal velocities at medium and maximum resolutions.

Panels C, D in Fig. 13 compare the u-velocities from several Test B calculations using the two second-order models in comparison with first-order P1-E0 model results from Fig. 3. Each panel shows results from the upper surface ($\sigma = 100\%$) in solid lines and results from a surface a quarter of the way up from the bottom ($\sigma = 25\%$) in dashed lines. Panel C shows results from medium resolution calculations ($r = 8, 20$ in the second-order and first-order calculations, respectively) and panel D shows the corresponding results from the higher resolution calculations ($r = 16, 40$). At these resolutions the accuracy of the first- and second-order calculations is very similar so for clarity the second-order results are displaced horizontally from the first-order results by 0.05 nondimensional units. The P2-E1 results in magenta are displaced to the left and the P2-P1 results in blue are displaced to the right. In general, models satisfying the solvability condition, namely the P1-E0 and P2-E1 models, are better behaved than the P2-P1 model. This is possibly related to the well-known "weak" mass conservation of the Taylor-Hood element. This problem is greatly improved by "enriching" the pressure

August 30, 2024

993   space with constant pressures in each triangular element (Boffi et al., 2012). In the 2D

994   Test B problem this increases the number of pressure variables from $n_p = n(m+1)$ in the

995   basic Taylor-Hood element to $n(3m+1)$, much closer to the $4nm$ needed to satisfy the

996   solvability condition. On the other hand, the pressure in the P2-E1 case is highly

997   oscillatory but well behaved in the P2-P1 case. However, this is not at all concerning

998   since the transformed pressure, a Lagrange multiplier, has no physical significance.

999

1000   **8. A Summary and Discussion**

1001

1002   In summary, this paper presents two innovations in ice sheet modeling. The first involves

1003   a transformation of the ice sheet Stokes equations into a form that differs from the

1004   approximate Blatter-Pattyn system by a small number of terms. In particular, the

1005   variational formulations differ only by the absence of terms involving the vertical

1006   velocity w in the second invariant of the strain rate tensor in the Blatter-Pattyn system.

1007

1008   We focus on two applications of the new transformation. The first is that these

1009   extra terms in the transformed Stokes equations may be "switched" on or off to convert

1010   the code from a full-Stokes model to a Blatter-Pattyn model, if desired. Ice sheet flow is

1011   generally shallow but often contains limited areas where Stokes equations must be

1012   solved. Thus, the switch from Blatter-Pattyn to Stokes may be done locally and

1013   adaptively only where the extra accuracy is required.

1014

1015   The fact that neglecting the vertical velocity in only one localized place creates

1016   the Blatter-Pattyn approximation suggests that approximating the vertical velocity instead

1017   will create improved approximations. We present two such approximations. The first

1018   approximation, called the BP+ approximation, solves the pressure-free horizontal

1019   momentum equation with the vertical velocity obtained from the continuity equation.

1020   Remarkably, this approximation turns out to be the same as a model originally proposed

1021   by Herterich (1987). An intriguing idea would be to replace the BP with the BP+

1022   approximation in the adaptive switching method. The second approximation simply

1023   approximates the vertical velocity by discretizing the continuity equation on a coarser

1024   grid than the rest of the model.

1025

1026   The second innovation involves the introduction and use of finite element

1027   discretizations that feature a decoupled invertible continuity equation permitting the

1028   numerical solution for the vertical velocity in terms of the horizontal velocity

1029   components, i.e., $w = w(u,v)$. Some examples of such grids for use in 2D and 3D are

1030   given in Appendix B. An important example is the P1-E0 grid that is used in most of the

1031   test problems in this paper. However, one can alternatively obtain $w = w(u,v)$ by other

1032   means, as for example by discretizing (43). For example, this is done in MALI (Hoffman

1033   et al., 2018), a code based on the Blatter-Pattyn approximation, to obtain the vertical

1034   velocity w for the advection of ice temperature (Mauro Perego, private communication).

1035

1036   Finally, no cost comparisons have been presented because the present calculations

1037   are only proof of concept, made on a personal computer using the program Mathematica.

1038   This is not at all representative of the computer hardware or the methods used in practical

1039   ice sheet modeling. Furthermore, no effort was made to optimize the calculations or to

1040   take advantage of parallelization. As a result, cost comparisons would be inaccurate and

1041   possibly misleading.

1042

1043   **Code Availability**

1044

1045   All calculations were made using the Wolfram Research, Inc. program Mathematica in a

1046   development environment. No production code is available.

1047

1048   **Competing Interests**

1049

1050   The author has acknowledged that there are no competing interests.

1051

1052   **Acknowledgements**

1053

1057

August 30, 2024

References

Auricchio, F., da Veiga, L.B., Brezzi, F., and Lovadina, C.: Mixed Finite Element Methods, In Encyclopedia of Computational Mechanics Second Edition (Eds E. Stein, R. de Borst, and T.J.R. Hughes), John Wiley & Sons, Ltd., 2017.

Blatter, H.: Velocity and Stress Fields in Grounded Glaciers: A Simple Algorithm for Including Deviatoric Stress Gradients, J. Glaciol., 41, 333-344, 1995.

Boffi, D., Brezzi, F., Fortin, M.: Finite Elements for the Stokes Problem. In: Boffi D., Gastaldi L. (eds) Mixed Finite Elements, Compatibility Conditions, and Applications. Lecture Notes in Mathematics, vol 1939. Springer, Berlin, Heidelberg. https://doi.org/10.1007/978-3-540-78319-0_2, 2008.

Boffi, D., Cavallini, N., Gardini, F., and Gastaldi, L.: Local Mass Conservation of Stokes Finite Elements, J. Sci. Comput., 52, 383–400, 2012.

Chen, Q., Gunzburger, M., and Perego, M.: Well-Posedness Results for a Nonlinear Stokes Problem Arising in Glaciology, SIAM J. Math. Anal., 45(5), 2710-2733, 2013.

Cheng, G., Lötstedt, P., and von Sydow, L.: A Full Stokes Subgrid Scheme in Two Dimensions for Simulation of Grounding Line Migration in Ice Sheets Using Elmer/ICE (v8.3), Geosci. Model Dev., 13, 2245-2258, 2020.

Dukowicz, J.K., Price, S.F., and Lipscomb, W.H.: Consistent Approximations and Boundary Condition for Ice Sheet Dynamics from a Principle of Least Action, J. Glaciol., 56, 480-496, 2010.

Dukowicz, J.K., Price, S.F., and Lipscomb, W.H.: Incorporating Arbitrary Basal Topography in the Variational Formulation of Ice Sheet Models, J. Glaciol., 57, 461-467, 2011.

Dukowicz, J.K.: Refolmulating the Full-Stokes Ice Sheet Model for a More Efficient Computational Solution, The Cryosphere, 6, 21-34, 2012.

August 30, 2024

1093 Elman, H.C., D.J. Silvester, and A.J. Wathen, 2014: *Finite Elements and Fast Iterative*
1094 *Solvers: With Applications in Incompressible Fluid Dynamics*, 2nd Ed., Oxford
1095 University Press, 494 pp.

1096

1097 Gagliardini, O., and Zwinger, T.: The ISMIP-HOM Benchmark Experiments Performed
1098 Using the Finite-Element Code Elmer, The Cryosphere, 2, 67–76, 2008.

1099

1100 Gagliardini, O., Zwinger, T., Gillet-Chaulet. F., Durand, G., Favier, L., de Fleurian, B.,
1101 Greve, R., Malinen, M., Martín, C., Råback, P., Ruokolainen, J., Sacchettini, M., Schäfer,
1102 M., Seddik, H., and Thies, J.: Capabilities and Performance of Elmer/Ice, a New-
1103 Generation Ice Sheet Model, Geosci. Model Dev., 6, 1299–1318, doi:10.5194/gmd-6-
1104 1299-2013, 2013.

1105

1106 Greve, R. and Blatter, H.: Dynamics of Ice Sheets and Glaciers, Springer-Verlag, Berlin
1107 Heidelberg, 2009.

1108

1109 Heinlein, A., Perego, M., and Rajamanickam, S.: FROSch Preconditioners for Land Ice
1110 Simulations of Greenland and Antarctica, SIAM J. Sci. Comput., 44, V339-B367, doi:
1111 10.1137/21M1395260, 2022.

1112

1113 Herterich, K.: On the Flow Within the Transition Zone Between Ice Sheet and Ice Shelf,
1114 in Dynamics of the West Antarctic Ice Sheet, Proceedings of a workshop held in Utrecht,
1115 May 6-8, 1985, (Eds. C. J. Van Der Veen and J. Oerlemans), D. Reidel, Dordrecht, 185-
1116 202, 1987.

1117

1118 Hoffman, M. J., Perego, M., Price, S. F., Lipscomb, W. H., Zhang, T., Jacobsen, D.,
1119 Tezaur, I., Salinger, A. G., Tuminaro, R., and Bertagna, L.: MPAS-Albany Land Ice
1120 (MALI): A Variable-Resolution Ice Sheet Model for Earth System Modeling Using
1121 Voronoi Grids, Geosci. Model Dev.*, 11, 3747–3780, doi:10.5194/gmd-11-3747-2018,
1122 2018.

1123

1124 Hood, P. and Taylor, C.: Numerical Solution of the Navier-Stokes Equations Using the
1125 Finite Element Technique, Comput. Fluids, 1, 1-28, 1973.

1126

1127 Larour, E., Seroussi, H., Morlighem, M., and Rignot, E.: Continental scale, high order,

1128 high spatial resolution, ice sheet modeling using the Ice Sheet System Model (ISSM), J.

1129 Geophys. Res., 117, 1–20, doi:10.1029/2011JF002140, 2012.

1130

1131 Leng, W., Ju, L., Gunzburger, M., Price, S., and Ringler, T.: A Parallel High-Order

1132 Accurate Finite Element Nonlinear Stokes Ice Sheet Model and Benchmark Experiments,

1133 J. Geophys. Res., 117, 2156–2202, doi:10.1029/2011JF001962, 2012.

1134

1135 Lipscomb, W.H., Price, S.F., Hoffman, M.J., Leguy, G.R., Bennett, A.R., Bradley, S.L.,

1136 Evans, K.J., Fyke, J.G., Kennedy, J.H., Perego, M., Ranken, D.M., Sacks, W.J., Salinger,

1137 A.G., Vargo, L.J., and Worley, P.H.: Description and Evaluation of the Community Ice

1138 Sheet Model (CISM) v. 2.1, Geosci. Model Dev., 12, 387-424, 2019.

1139

1140 Nowicki, S.M.J. and Wingham, D.J.: Conditions for a Steady Ice Sheet-Ice Shelf

1141 Junction, *Earth Planet. Sci. Lett.*, **265**(1-2), 246-255, 2008.

1142

1143 Pattyn, F.: A New Three-Dimensional Higher-Order Thermomechanical Ice Sheet

1144 Model: Basic Sensitivity, Ice Stream Development, and Ice Flow across Subglacial

1145 Lakes, J. Geophys. Res., 108(B8), 2382, 2003.

1146

1147 Pattyn, F., Perichon, L., Aschwanden. A., Breuer, B., de Smedt, B., Gagliardini, O.,

1148 Gudmundsson, G.H., Hindmarsh, R.C.A., Hubbard, A., Johnson, J.V., Kleiner, T.,

1149 Konovalov, Y., Martin, C., Payne, A.J., Pollard, D., Price, S., Ruckamp, M., Saito, F.,

1150 Soucek, O., Sugiyama, S., and Zwinger, T.: Benchmark Experiments for Higher-Order

1151 and Full-Stokes Ice Sheet Models (ISMIP–HOM*),* The Cryosphere, 2, 95-108, 2008.

1152

1153 Perego, M., Gunzburger. M., and Burkardt, J.: Parallel Finite-Element Implementation

1154 for Higher-Order Ice-Sheet Models, J. Glaciol., 58, 76-88, 2012.

1155

1156 Rückamp, M., Kleiner, T., and Humbert, A.: Comparison of ice dynamics using full-

1157 Stokes and Blatter-Pattyn approximation: application to the Northeast Greenland Ice

1158 Stream, The Cryosphere, 16, 1675-1696, 2022.

August 30, 2024

1159

1160   Schoof, C.: Coulomb friction and other sliding laws in a higher order glacier flow model,

1161   Math. Models. Meth. Appl. Sci., 20(1), 157–189, 2010.

1162

1163   Schoof, C. and Hewitt, I.: Ice-Sheet Dynamics, Annu. Rev. Fluid Mech., 45, 217–239,

1164   2013.

1165

1166   Schoof, C. and Hindmarsh, R.C.A.: Thin-Film Flows with Wall Slip: An Asymptotic

1167   Analysis of Higher Order Glacier Flow Models, Quart. J. Mech. Appl. Math, 63, *73-114*,

1168   2010.

1169

1170   Seroussi, H., Ben Dhia, H., Morlighem, M., Latour, E., Rignot, E., and Aubry, D.:

1171   Coupling Ice Flow Models of Varying Orders of Complexity with the Tiling Method, J.

1172   Glaciol., 58, 776-786, 2012.

1173

1174   Tezaur, I. K, Perego, M., Salinger, A. G., Tuminaro, R. S., and Price, S. F.:

1175   Albany/FELIZ: A Parallel, Scalable and Robust, Finite Element, First-Order Stokes

1176   Approximation Ice Sheet Solver Built for Advanced Analysis, Geosci. Model Dev., 8,

1177   1197-1220, 2015.

1178

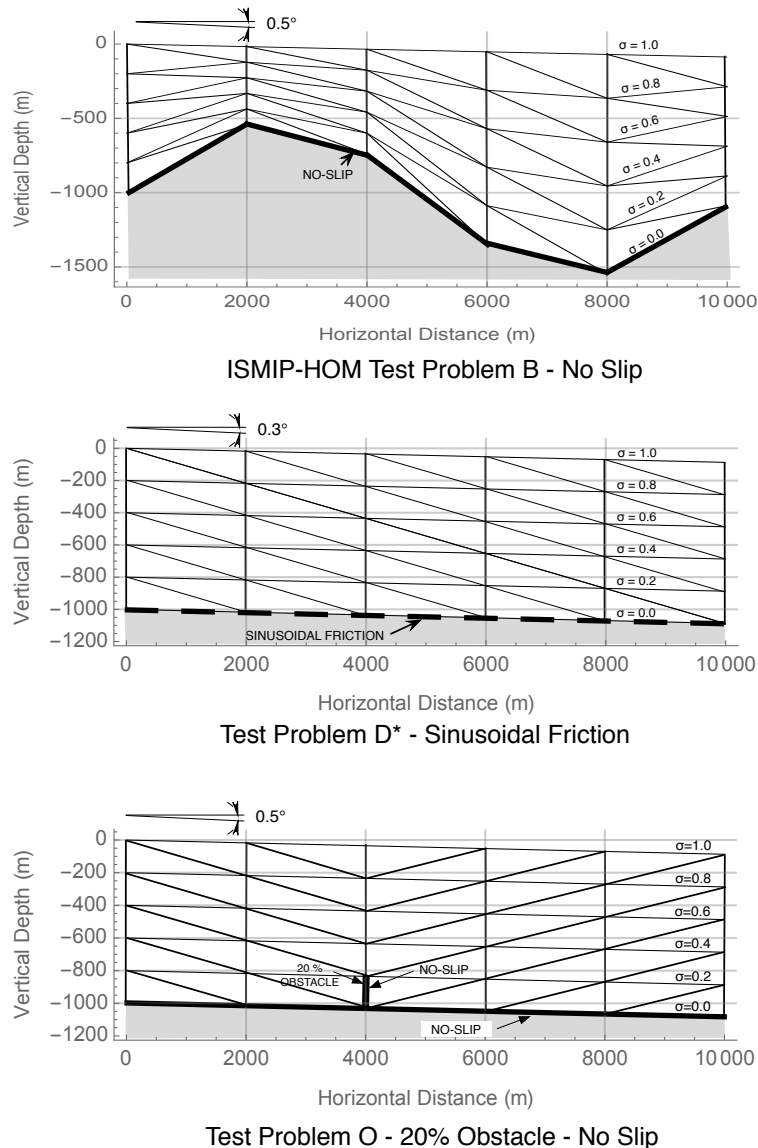1179   **Appendix A: Test Problems**

1180

1181   We will use three 2D test problems to demonstrate the new methods. The geometrical

1182   configuration of the three problem grids is illustrated in Fig. A1. The first problem, Test

1183   B, is actually Exp. B from the ISMIP-HOM benchmark suite (Pattyn et al., 2008); it

1184   features a no-slip condition (infinite friction) on a sinusoidal basal surface. The second

1185   problem, Test D*, incorporating sinusoidal friction along a uniformly sloped plane basal

1186   surface, is a replacement with modified parameters for Exp. D from the benchmark suite

1187   since ice flow in Exp. D is nearly vertically uniform (see Fig. 4), more characteristic of a

1188   shallow-shelf approximation, and this is rectified by increased basal friction.

1189

1190   A third problem, Test O (for "Obstacle") is introduced to the illustrate adaptive

1191   switching discussed in §6.1. Test O has a unique feature, namely, a thin no-slip obstacle,

1192   located at $x = 4\,km$ and extending vertically $200\,m$ from the bed (20 % of the ice sheet

1193   thickness), as illustrated in Fig. A1, which forces the ice flow near the obstacle to adjust

1194 abruptly. Because of the no-slip boundary conditions along the obstacle surface, a

1195 triangular element in the lee of the obstacle, with one vertical edge and one edge along

1196 the bed, would have all zero vertex velocities. This implies zero stress and therefore a

1197 local singularity in ice viscosity. To avoid this, all elements at the back of the obstacle

1198 are "reversed" as compared to the ones at the front of the obstacle, as shown in Fig. A1.

1199

ISMIP-HOM Test Problem B - No Slip

Test Problem D* - Sinusoidal Friction

Test Problem O - 20% Obstacle - No Slip

1200

1201 **Figure A1.** Test problem grids. For clarity, a coarse 5x5 configuration is shown.

1202

1203 All tests feature a sloping flat upper surface, given by $z_s(x) = -x \operatorname{Tan}(\theta)$, where

1204 $\theta = 0.5°$ for Tests B and O, and $\theta = 0.3°$ for Test D* (this differs from the $0.1°$ slope in

1205 Test D), with a free-stress upper boundary condition in all cases. The sinusoidal bottom

August 30, 2024

1206   surface elevation for Test B is specified by $z_b(x) = z_s(x) - H_0 + H_1 \text{Sin}(\omega x)$, where the

1207   depth $H_0 = 1000\,m$, $H_1 = 500\,m$, $\omega = 2\pi/L$, and L is the perturbation wavelength,

1208   which is also the domain length. The bottom surface elevation in Tests D* and O is

1209 $z_b(x) = z_s(x) - H_0$, parallel to the upper surface. The length L in the ISMIP-HOM suite

1210   ranges from $5\,km$ to $160\,km$, but here we consider only the two cases at the high end of

1211   the aspect ratio H_0/L range, namely, $L = 5\,km$ and $L = 10\,km$, where the inaccuracy of

1212   the Blatter-Pattyn approximation becomes noticeable. In all cases the lateral boundary

1213   conditions are periodic. The spatially varying friction coefficient for Test D* is given by

1214 $\beta(x) = \beta_0 + \beta_1 \text{Sin}(\omega x)$, where $\beta_0 = \beta_1 = 10^4\,Pa\,a\,m^{-1}$ (these are an order of magnitude

1215   higher than in Test D). The physical parameters are the same as in ISMIP-HOM,

1216   namely, ice-flow parameter $A = 10^{-16}\,Pa^{-3}a^{-1}$, ice density $\rho = 910\,kg\,m^{-3}$, and

1217   gravitational constant $g = 9.81\,ms^2$. In general, units are MKS, except where time is

1218   given per annum, convertible to per second by the factor $3.1557 \times 10^7\,s\,a^{-1}$.

1219

1220   **Appendix B: Grids Satisfying the Solvability Condition**

1221   **B1 An Invertible Continuity Equation**

1222

1223   As discussed in §4, the invertibility of the discrete continuity equation requires special

1224   grids that satisfy the solvability condition. Here we discuss several such grids and their

1225   properties. Fig. B1 shows three 2D elements on triangles or quadrilaterals that satisfy the

1226   solvability condition (57) in certain circumstances. The P1-E0 element is quite general,

1227   as demonstrated in §B2. It has velocities located at triangle vertices, resulting in a linear

1228   velocity distribution within each triangle (P1), and pressure located on the vertical edge

1229   of each triangle, providing a constant pressure over the two triangles that share that edge

1230   (E0). A second order version of this element, the P2-E1 element, is shown in Fig. 13A.

1231   The other two elements, the P1-Q0 and Q1-Q0 elements, satisfy the solvability condition

1232   when used in Tests B and D* but may not do so in other problems. The P1-Q0 element

1233   also has velocities on triangle vertices for a linear velocity distribution within each

1234   triangle (P1) but the pressure is constant within the quadrilateral (Q0) formed by the two

1235   adjoining triangles. The Q1-Q0 element has velocities located at quadrilateral vertices

1236   and pressure centered in the quadrilateral, resulting in a bi-quadratic velocity distribution

1237   (Q1) and a constant pressure within the quadrilateral (Q0).

August 30, 2024
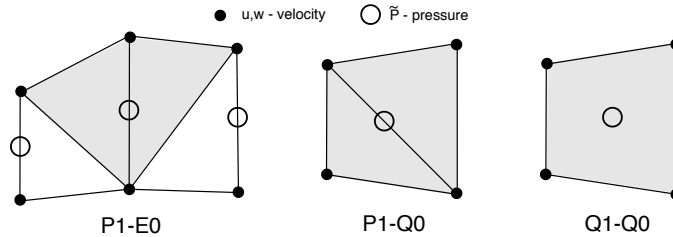
Figure B1. Three first-order 2D elements that may be used to satisfy the
solvability condition, (57), in Tests B and D[*].

The solutions are stable, as expected, and they all converge with the same value
for ice transport. The pressure distribution is smooth in the P1-E0 case, but contains
small fluctuations near the upper surface in the P1-Q0 and Q1-Q0 cases that tend to
disappear as resolution is increased. The Q1-Q0 element is unstable in conventional
applications because it contains a checkerboard pressure null space and is only used in a
stabilized form (see Elman et al., 2014, where the element is called Q1-P0). Here,
however, the Q1-Q0 grid does behave well, presumably because it satisfies the solvability
condition. Overall, this confirms our expectation of stability when the solvability
condition is satisfied. As we discuss next, the P1-E0 element is special because the
solvability condition is satisfied along each vertical edge, as opposed to being satisfied
over the entire grid as in the other two elements.

B2 The Solvability Condition in the P1-E0 Element

Fig. B2 illustrates the P1-E0 element used in a representative grid. We assume
that the grid is composed of vertical columns subdivided into triangular elements.
Consider a single vertical edge from bottom to the top. Assuming there are m edge
segments in the vertical direction, there will be $m+1$ discrete w variables and m discrete
$\tilde{P}$ variables since each $\tilde{P}$ variable is located between a pair of w variables. However,
since the w variable at the bed is specified as a boundary condition, either directly as a
no-slip condition or as part of a no-penetration condition, there will be only m unknown
w variables. As a result we have $n_w = n_p$ along each vertical grid edge, and therefore
over the entire grid, satisfying the solvability condition. In case Lagrange multipliers are
used, there will be $m+1$ unknown discrete w variables (since now the basal vertical
velocity w is also an unknown). However, this is matched by m unknown $\tilde{P}$ variables,
supplemented by one λ_z or one Λ unknown Lagrange multiplier variable, depending on
the type of boundary condition. Thus, again the number of unknown variables equals the

August 30, 2024

1268   number of equations along every vertical edge, thereby satisfying the solvability

1269   condition whether Lagrange multipliers are used or not. This means that the P1-E0

1270   element can be used to satisfy the solvability condition irrespective of the boundary

1271   conditions on quite arbitrary grids, as illustrated in Fig. B2. These arguments apply for

1272   other versions of the P1-E0 element as well, such as the second order version P2-E1 in

1273   Fig. 13A or the 3D version in Fig. B3.
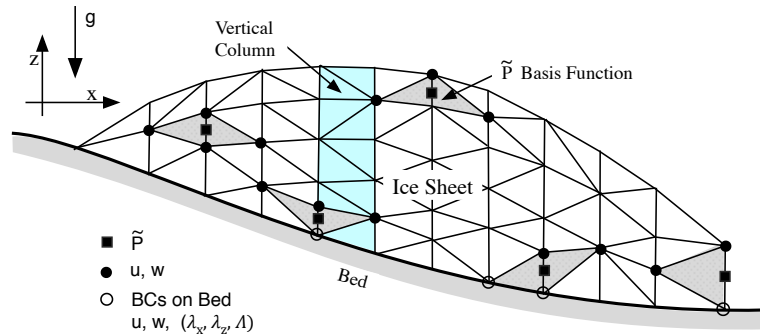
1274

1275

Figure B2. An illustration of a 2D edge-based P1-E0 grid, composed of vertical columns

1277   randomly subdivided into triangles. Pressures are located on the vertical edges.

1278   The triangulation and the configuration of the associated pressure basis functions

1279   (shown in gray) is quite general, allowing for a flexible triangulation of the domain.

1280

B3 Two- and Three-Dimensional Meshes Based on the P1-E0 Element

1282   The P1-E0 element has been used on the test problem grids in Fig. A1 and

1283   performs well. Moreover, the element has great geometric generality, as in Fig. B2, so it

1284   may be used for quite complicated grids. Generally, there are two triangles associated

1285   with a pressure variable, one on each side of a vertical edge, except in situations where

1286   the ice sheet ends at a vertical face, as in Fig. B2. However, there is no problem since the

1287   pressure is simply associated with the single triangle on one side of the vertical face.

1288

1289   Meshes composed of P1-E0 elements have another useful property. Since

1290   pressure and vertical velocity variables alternate along vertical grid lines, the matrix-

1291   vector products $M_{WP}\,p$, $M_{WP}^{T}\,w$ in (47), corresponding to $\partial\tilde{P}/\partial z$ and $\partial w/\partial z$ in the

1292   vertical momentum and continuity equations, respectively, consist of simple decoupled

1293   bi-diagonal one-dimensional difference equations along each vertical grid line for

1294   determining pressure and vertical velocity. This should be particularly advantageous for

1295   parallelization.

1296

1297   The two-dimensional P1-E0 element has a relatively simple three-dimensional

1298   counterpart, shown in Fig. B3. The mesh again consists of vertical columns, this time

1299   composed of hexahedra. Each hexahedron is subdivided into six tetrahedra such that

1300   each vertical edge is surrounded by as few as four to as many as eight tetrahedra. As in

1301   the 2D case, velocity components are collocated at vertices, yielding a piecewise-linear

1302   velocity distribution in each tetrahedral element, and pressures are located in the middle

1303   of each vertical edge so that pressure is constant in the tetrahedra that surround that edge.

1304   Lagrange multipliers, if used, are located at the vertices on the basal surface, yielding a

1305   piecewise linear distribution on the basal triangular facet. Since pressures and vertical

1306   velocities are again intermingled along a single line of vertical edges from top to bottom,

1307   we see that this satisfies the solvability condition (57) since the argument used in the 2D

1308   case applies here also.
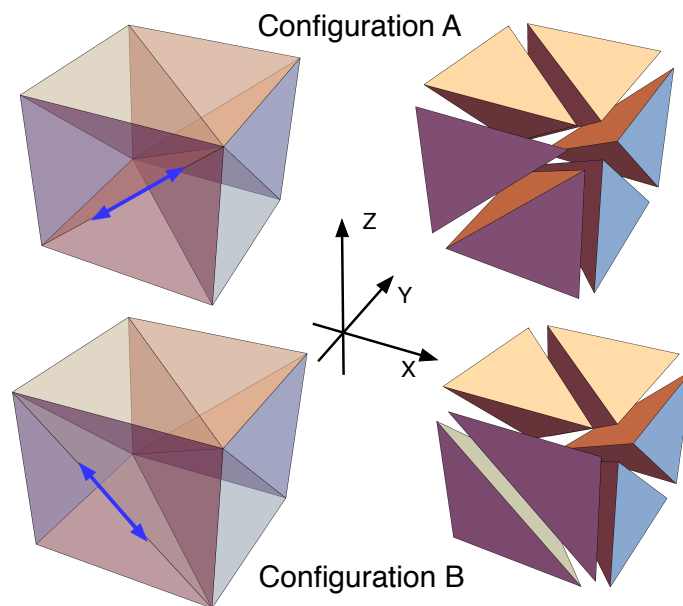
1309

1310   **Figure B3.** Three-dimensional P1-E0 tetrahedral elements that generalize the 2D

1311   P1-E0 element of Fig. C1. Configurations A and B differ by having an internal

1312   triangular face rotated, as indicated by the blue arrows. Both configurations

1313   satisfy the solvability condition.

1314

1315   Fig. B3 shows two of the several possible configurations of a typical hexahedron,

1316   including an exploded view of each configuration for clarity. The two configurations

1317   differ in having the internal face of the two forward-facing tetrahedra rotated, creating

1318   two different forward facing tetrahedra. The remaining six tetrahedra are undisturbed.

August 30, 2024

1319 Since edges must align when hexahedra (or tetrahedra) are connected, this showa that the

1320 3D mesh can be flexibly reconnected and rearranged, just as in the 2D case of Fig. B2.

1321

1322 **Remark #2**: A closely related but perhaps even simpler three-dimensional P1-E0

1323 element is one based on the P2-P1 prismatic tetrahedral element that is used in Leng et al.

1324 (2012). A grid of these elements is composed of vertical columns of triangular prisms,

1325 with triangular faces at the top and bottom, which are then each subdivided into three

1326 tetrahedra. As in Fig. B3, pressures are located on the vertical prism edges so this again

1327 satisfies the solvability condition.

1328

1329   Just as the 2D second-order P2-E1 element in Fig. 13A is a generalization of the

1330 P1-E0 element, a 3D second-order P2-E1 element may be constructed as a generalization

1331 of the P1-E0 element illustrated in Fig. B3. Velocities would be located at the vertices

1332 and at midpoints of the tetrahedral edges, and pressures halfway between the velocities

1333 on vertical edges, including the imaginary vertical edges through the midpoints of the

1334 tetrahedral edges, in the same way as in the 2D case in Fig. 13A. The P2-E1 element in

1335 both 2D and 3D would also satisfy the solvability condition since the arguments in §B2

1336 apply here as well because pressures are again located midway between vertical

1337 velocities along all vertical edges.